arXiv:cond-mat/0607676v1 [cond-mat.supr-con] 26 Jul 2006

Chapter 1

Vortex state microwave response in superconducting cuprates and MgB_2

E. Silva[†], **N. Pompeo**[‡], **S. Sarti**[§], **C. Amabile**[¶]

[†] *Dipartimento di Fisica "E. Amaldi" and Unità CNISM,*
Università Roma Tre, Via della Vasca Navale 84, 00146 Roma, Italy

e-mail: silva@fis.uniroma3.it

[‡] *Dipartimento di Fisica "E.Amaldi" and Unità CNISM, Università*
Roma Tre, Via della Vasca Navale 84, 00146 Roma, Italy

[§] *Dipartimento di Fisica and Unità CNISM,*
Università "La Sapienza", P.le Aldo Moro 2, 00185 Roma, Italy

e-mail: stefano.sarti@roma1.infn.it

[¶] *Dipartimento di Fisica,*
Università "La Sapienza", P.le Aldo Moro 2, 00185 Roma, Italy

Abstract

We investigate the physics of the microwave response in $YBa_2Cu_3O_{7-\delta}$, $SmBa_2Cu_3O_{7-\delta}$ and MgB_2 in the vortex state. We first recall the theoretical basics of vortex-state microwave response in the London limit. We then present a wide set of measurements of the field, temperature, and frequency dependences of the vortex state microwave complex resistivity in superconducting thin films, measured by a resonant cavity and by swept-frequency Corbino disk. The combination of these techniques allows for a comprehensive description of the microwave response in the vortex state in these innovative superconductors. In all materials investigated we show that flux motion alone cannot take into account all the observed experimental features, neither in the frequency nor in the field dependence. The discrepancy can be resolved by considering the (usually neglected) contribution of quasiparticles to the response in the vortex state. The peculiar, albeit different, physics of the superconducting materials here considered, namely two-band superconductivity in MgB_2 and superconducting gap with lines of nodes in cuprates, give rise to a substantially increased contribution of quasiparticles to the field-dependent microwave response. With careful combined analysis of the data it is possible to extract or infer many interesting quantities related to the vortex state, such as the temperature-dependent characteristic vortex frequency and vortex viscosity, the field dependence of the quasiparticle density, the temperature dependence of the σ-band superfluid density in MgB_2

Keywords: superconductivity, surface impedance, microwaves, vortex motion, cuprates, $YBa_2Cu_3O_{7-\delta}$, $SmBa_2Cu_3O_{7-\delta}$, MgB_2, vortex viscosity.

1.1 INTRODUCTION

One of the most versatile experimental methods for the investigation of the physics of superconductors is the measurement of the complex response to an alternating electromagnetic (e.m.) field in the radiofrequency (*rf*) and microwave ranges. The resulting data have been of great help in the understanding of the physics of conventional superconductors. Even confining the treatment to the linear response, in conventional superconductors microwave or *rf* measurements allowed, e.g., for the determination of the existence [1] and temperature dependence [2] of the superconducting gap, for the settling of the kind of dynamical fluctuations [3, 4, 5], for the determination of the penetration depth [6, 7, 8], for the determination of the thermodynamical critical field and of the third critical field for surface superconductivity [9], and for the determination of the upper critical field [10].

In type-II superconductors the investigation was extended to the mixed state: when the magnetic field $H_{c1} < H < H_{c2}$, with H_{c1} and H_{c2} the temperature dependent lower and upper critical field, respectively, the magnetic flux penetrates the superconductor as quantized flux lines, each carrying one flux quantum $\Phi_0 = 2.07\times10^{-15}$ T·m^2. Such flux lines, in presence of an electric current density $\mathbf{J}$, are subjected to a Lorentz force (per unit length) $\mathbf{F_L} = \mathbf{J} \times \mathbf{\Phi_0}$ (where $\mathbf{\Phi_0} \parallel \mathbf{B}$). Moving vortices dissipate energy, so that an ideal type-II superconductor always has a finite resistivity in the vortex state. Dissipation can be viewed either as due to the continuous conversion of Cooper pairs into quasiparticles at the (moving) vortex boundary [11], or to Joule heating inside of the vortex core [12, 13]. In any case, the dissipation is expected to depend mainly on the fundamental properties of the superconductors, such as the quasiparticle density of states and relaxation time in the vortex core, and thus it is expected to be very similar in different samples of the same material.

A dissipationless regime can be achieved in dc by pinning vortices to defects [14, 15, 16]. When the force acting on vortices is alternating, pinning determines an additional imaginary (out-of-phase) response. As opposed to energy dissipation, the particular pinning mechanism and its efficacy are expected to be strongly sample dependent.

To take into account the energy dissipation and the effects of pinning a simple way is to build up an equation of motion for a single vortex. In a simple model, independently pinned vortices are considered and the equation of motion for the displacement $\mathbf{u}$ from the equilibrium position is written in the elastic approximation[1]: $\eta\dot{\mathbf{u}} + \kappa_p\mathbf{u} = \mathbf{F_L}$, where η is the so-called *vortex viscosity* (per vortex unit length) and takes into account the energy dissipation, and κ_p is the *pinning constant* (per vortex unit length) and takes into account the pinning of vortices. This simple equation of motion gives rise to a complex vortex motion resistivity due to an alternating current density $\mathbf{J}e^{\mathrm{i}\omega t}$, with $\nu = \omega/2\pi$ the measuring frequency, that can be written as [22]:

$$\rho_{vGR} = \frac{\Phi_0 B}{\eta}\frac{1}{1-\mathrm{i}\frac{\kappa_p}{\eta\omega}} = \rho_{ff}\frac{1}{1-\mathrm{i}\frac{\omega_p}{\omega}} \tag{1.1}$$

where the last equality defines the so-called *flux-flow resistivity*, ρ_{ff}, and the *depinning frequency* (sometimes called "pinning frequency") $\nu_p = \omega_p/2\pi$. Referring to the physical meaning of the vortex parameters, η is expected to be a very similar, if not universal, function of the external parameters (e.g., the temperature) in different samples of the same material: it is a quantity related to the fundamentals of the physics of type-II superconductors. In particular, it was demonstrated by Bardeen and Stephen (BS) [13] that,

---

[1] The vortex mass is usually neglected [17, 18], even if this is still a debated topic [19, 20, 21].

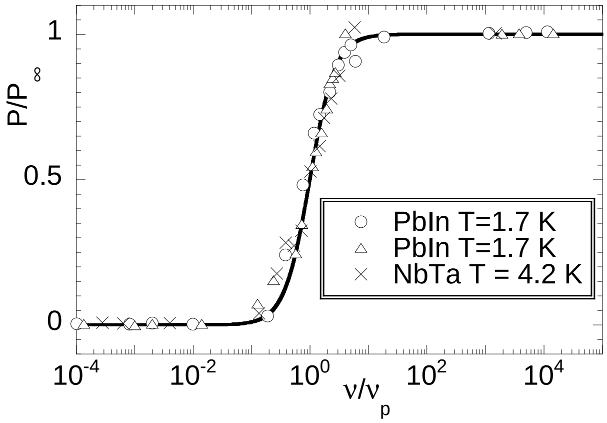

Figure 1.1: Normalized dissipated power in type-II superconductors at $H = \frac{1}{2}H_{c2}$ as a function of the measuring frequency normalized to ν_p (replotted from [22]) and fit by Eq.(1.1). ν_p = 3.9, 5.1, 15 MHz [22].

in dirty superconductors, $\eta = \Phi_0 B_{c2}/\rho_n$, where ρ_n is the normal state dc resistivity and B_{c2} is the upper critical field.

In deep contrast, one expects largely different magnitudes, temperature and magnetic field dependence for κ_p (or ω_p) in different samples even of the same material, being the pinning constant related to extrinsic properties. Its study can, on one side, shed light on the characteristic features of the vortex matter, and on the other side can be of essential importance for the applications of superconductors [14, 15, 16].

The applicability of Eq.(1.1) was first brought to the attention of the scientific community with the seminal paper by Gittleman and Rosenblum [22]: as shown in Fig.1.1, the data for the dissipated power ($\propto$ Re[ρ_{vGR}]) in thin superconducting films followed very closely Eq.(1.1) over several orders of magnitude for the measuring frequency. The success of this extremely simple model determined its assumption for the interpretation of the data taken in high-T_c superconductors (HTCS). Many studies were carried out in HTCS, aimed at the determination of the vortex viscosity and pinning constant through measurements of the radiofrequency, microwave or millimeter-wave response [23, 24, 25, 26, 27, 28, 29, 30, 31, 32, 33, 34, 35, 36, 37, 38, 39, 40, 41, 42, 43, 44]. In particular, in the most studied compound $YBa_2Cu_3O_{7-\delta}$ (YBCO), it was found that the depinning frequency was located in the GHz range, thus making microwave techniques the ideal candidate method for the experimental investigation of the vortex motion. However, even after many years from the discovery of YBCO, the values given for vortex parameters as determined by microwave measurements (see [35] for a clear overview) presented a very puzzling framework. As reported in Figs.1.2 and 1.3, with

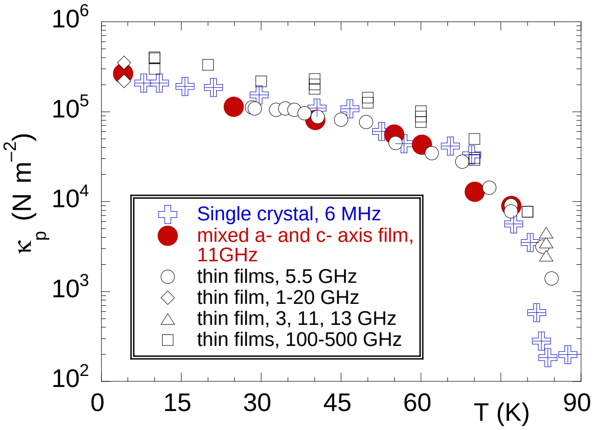

Figure 1.2: Pinning constant κ_p for many different YBCO samples: [23], crosses; [28], red full dots; [30], open circles; [31], diamonds; [33], open squares; [34], triangles. Data replotted from original papers. A remarkable collapse of the data on a single curve is evident.

data replotted from original papers [23, 27, 28, 30, 31, 32, 33, 34] cited in [35], it was shown that while data for κ_p taken on different samples (c-axis and mixed a- and c- axis films from various sources, single crystals) lie all together on the same curve, the vortex viscosity presented a wide scattering of the data. As discussed above, due to the meaning of the vortex parameters this finding is not easily explained: one would rather expect, for a given material, a universal behavior for η and a sample-dependent k_p.

Similar oddities were systematically evident also in different frequency ranges in various HTCS. Sub-THz measurements of the vortex-state microwave resistivity of thin YBCO films [33] showed that vortex parameters obtained from conventional, vortex-motion-driven response, were in strong contrast with calculations of the same parameters from microscopic theories. Again, the pinning constant was found nearly sample-independent. The apparent vortex viscosity would differ from the microscopic calculation by more than an order of magnitude. An alternative analysis of the data [45] suggested that it was not possible to ignore, in the interpretation of the data, the effect of field-induced pair breaking. Accordingly to that picture, data of the imaginary conductivity in the same frequency range in $Bi_2Sr_2CaCu_2O_{8+x}$ (BSCCO) films in the vortex state [46] could be accounted for even without resorting to any vortex motion model, being the field-induced superfluid density suppression sufficient for a quantitative description.

Summarizing, it was clear that Eq.(1.1) did not provide a comprehensive explanation of the vortex state microwave response in HTCS. Even if

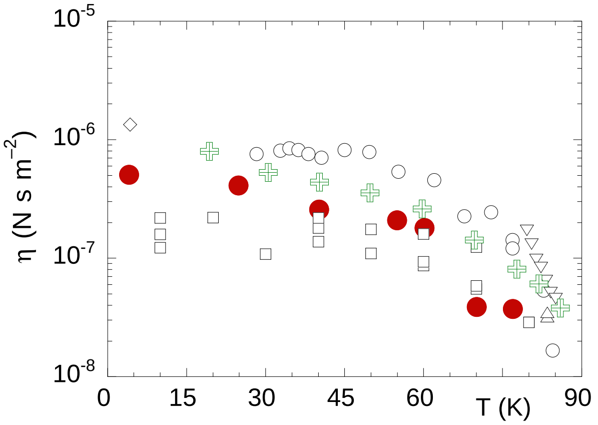

Figure 1.3: Vortex viscosity η for many different YBCO samples: [27], down triangles; [28], red full dots; [30], open circles; [31], diamonds;[32], crosses; [33], open squares; [34], triangles. Data replotted from original papers. A remarkable spread of the data is evident.

much more complicated (and probably more realistic) vortex models could be invoked [47, 48], additional mechanisms had to be investigated.

Granularity has been sometimes indicated as a possible dominant source for the losses in the microwave response in superconducting films. Manifestations of granularity include weak-links dephasing [49, 50, 51, 52, 53, 54, 55], Josephson fluxon (JF) dynamics [56] and, as recently studied, Abrikosov-Josephson fluxon (AJF) dynamics [57, 58]. Weak-links dephasing is characterized by a very sharp increase of the dissipation at dc fields of order of, or less than, 20 mT, accompanied by a strong (and sometimes exceptionally strong) hysteresis with increasing or decreasing field [49, 50, 51, 52]. However, those effects are relevant in large-angle grain boundaries (or very weak links), such as those found in pellets and granular samples, and are not observed in good thin films. Josephson fluxon dynamics has been studied essentially in relation to nonlinear effects [59, 60], due to the short JF nucleation time. One of the characteristic features of AJF should be a rather pronounced sample dependence (defect-driven) of the microwave response, as in fact reported in Tl-2212 films [61]. This fact contrasts with the pseudo-universal behavior of the estimated κ_p, even if contributions from AJF cannot in general be excluded *a priori*.

Another intrinsic, unavoidable source for the measured microwave resistivity is obviously the conductivity due to charge carriers, that we write in terms of the so-called "two-fluid model" [11]: charge carriers are thought as given by a superconducting fraction x_s and a "normal" fraction (more appropriately, due to quasiparticle excitations) x_n. When the measuring frequency is much smaller than the quasiparticle relaxation rate this leads to the well-known dependence of the charge carriers conductivity at nonzero frequency:

$$\sigma = \sigma_1 - \mathrm{i}\sigma_2 = \frac{ne^2}{m\omega}\left(\omega\tau_{qp}x_n - \mathrm{i}x_s\right) = \frac{1}{\mu_0\omega}\left(\frac{2}{\delta_{nf}^2} - \mathrm{i}\frac{1}{\lambda^2}\right) \tag{1.2}$$

where n is the charge carrier density, m is the carrier effective mass, τ_{qp} is the quasiparticle scattering time, and the last equality defines the temperature, field and frequency dependent normal fluid skin depth δ_{nf} and the temperature and field dependent London penetration depth λ. How this charge carriers conductivity combines with the vortex motion resistivity is discussed in Section 1.2.

It should be mentioned that measurements of σ_1 and σ_2 in zero applied field have been demonstrated to be of crucial importance in the determination of the peculiarities of HTCS. As a partial list of examples, microwave measurements of the low-temperature variation of the superfluid fractional density, expressed as $x_s(T) = \left[\frac{\lambda(0)}{\lambda(T)}\right]^2$, have shown a clear nonactivated behavior in YBCO [62, 63], thus giving strong evidence for an anisotropic superconducting gap, with lines of nodes. In particular, a linear decrease with temperature was found in clean crystals [62, 63], demonstrating the existence of zero-energy excitations at low temperatures. Moreover, it was shown by microwave spectroscopy of the real part of the response in YBCO [64] that the quasiparticle relaxation rate $1/\tau_{qp}$ decreased, with respect to its value above T_c, by up to two orders of magnitudes. Short relaxation rates below T_c were confirmed in YBCO films by millimeter-wave interferometry [65], in YBCO crystals by surface resistance measurements [66], and in YBCO films by far-infrared measurements [67]. Crystals consistently presented $1/\tau_{qp}$ at low temperatures up to two order of magnitudes smaller than in the normal state [64, 66]. Similar drops were found in some films [65], while other films presented a difference in $1/\tau_{qp}$ of only a factor of two [67].

All the above mentioned mechanisms present novel features in the recently discovered [68] metallic superconductor MgB_2. The well-established, albeit sensitive to interband scattering, two-gap nature of this compound [69, 70, 71] is expected to strongly affect the intrinsic properties, and specifically to the present study, the vortex viscosity and the superfluid density. Microwave measurements [72, 73, 74] in zero dc magnetic field showed peculiar temperature dependences of the surface impedance, due to the existence of the double gap. Measurements of the magnetic-field-dependent microwave surface impedance [75, 76] at a single frequency presented very puzzling data for the vortex parameters, in particular strong field dependence of the vortex viscosity (or, using the Bardeen-Stephen model, for the upper critical field itself). These findings have their counterpart in other experimental and theoretical results: the London penetration depth was found theoretically to strongly depend on impurity level [77], thus giving an explanation for the large range of reported values. μSR spectroscopy data required for their satisfactory explanation that the application of a magnetic field induces a strong increase in the penetration depth at low fields [78], or at least that two different characteristic lengths [79] were involved. Moreover, it was theoretically shown [80] that the structure of vortices is very different in two-gap, with respect to single-gap, superconductors. To our knowledge, there are no exhaustive theories at present for what concerns the dynamics of vortices in multigap superconductors. There are however several experimental indications that a sufficiently strong magnetic field (of order 1 T) can quench the two-gap nature of MgB_2: scanning tunnel [81] and point-contact [82] spectroscopies showed that the superconductivity coming from the π band is strongly suppressed with the application of an external field $\sim$0.5 T. Neutron spectroscopy [83] brought evidence for a transformation of the vortex lattice at a similar field.

From all the above considerations it appears that, for different reasons, the microwave vortex state properties in YBCO (and, in general, in rare earth substituted materials RE-BCO) and MgB_2 are not yet unanimously understood. Aim of this study is to present microwave measurements at different frequencies and in wide magnetic field ranges, in order to identify the main fundamental mechanisms acting on the complex response. A related interest is to determine whether simple vortex motion models can be safely applied, possibly confining the complexity in some lumped parameter, or different approaches are needed.

This Chapter is organized as follows: Sec.1.2 presents an overview of the mean-field theory for vortex motion and two-fluid complex response, with some extension due to the peculiar electronic structure of the superconductors under study. Sec.1.3 presents the main properties of the samples under study, the electromagnetic response in thin films, and some detail on the resonant cavity and the Corbino disk employed for the measurements. Sec.1.4 presents and discusses the results in YBCO, MgB_2 and SmBCO. Conclusions are drawn in Sec.1.5.

1.2 THEORETICAL BACKGROUND

Considering an electromagnetic field incident on a flat interface between a generic medium and a bulk, thick (with respect to the penetration depth and skin depth) (super)conductor, the response to the field is given by the surface impedance Z_s [84]. Z_s equals the ratio between the tangential components of the alternating electric and magnetic fields, $Z_s = \frac{E_\parallel}{H_\parallel}$. This expression can be easily cast in the form $Z_s = \mathrm{i}\omega\mu_0\tilde{\lambda}$, being $\tilde{\lambda}$ an appropriate complex screening length. In the normal state, the screening length $\tilde{\lambda} \to \frac{\delta_n}{\sqrt{2\mathrm{i}}}$, where $\delta_n^2 = 2\rho_n/\mu_0\omega$ is the skin depth and ρ_n is the normal state resistivity. Deep in the superconducting state ($T \to 0$), the screening length is the London penetration depth λ. The complex response can be also described by a complex resistivity $\widetilde{\rho}$, related to the complex screening length $\tilde{\lambda}$ through the relation $\widetilde{\rho} = \mathrm{i}\omega\mu_0\widetilde{\lambda}^2$ (or equivalently to the surface impedance Z_s through the relation $Z_s = \sqrt{\mathrm{i}\omega\mu_0\widetilde{\rho}}$). Thus, the response can be expressed formally either by the surface impedance, the complex resistivity, the complex conductivity, or the complex screening length.

Many models have been developed and used for the frequency response in the vortex state, with various degrees of complexity [39, 85, 86, 87, 88, 89, 90, 91]. A very general expression for the surface impedance of a semi-infinite superconductor in the mixed state has been calculated [88], and later extended [92, 93, 94], by Coffey and Clem (CC) within the limit of validity of the two-fluid model (that is, in the local response limit). The result was expressed in terms of the combination of three complex screening lengths, related to the different contributions to the overall e.m. response: the superfluid response, given by the temperature and field dependent London penetration depth $\lambda(T, B)$; the normal fluid skin depth, given by $\delta_{nf}(T, B, \omega) = [2/\mu_0\omega\sigma_{nf}(T, B)]^{1/2}$ with σ_{nf} the quasiparticle conductivity; and the vortex response, given by the complex vortex penetration depth $\widetilde{\delta}_v(T, B, \omega) = [2\rho_v(T, B, \omega)/\mu_0\omega]^{1/2}$. The resulting expression for the surface impedance reads:

$$Z_s(T,B) = \mathrm{i}\omega\mu_0\widetilde{\lambda} = \mathrm{i}\omega\mu_0 \left(\frac{\lambda^2(T,B) - (\mathrm{i}/2)\widetilde{\delta}_v^2(B,T,\omega)}{1 + 2\mathrm{i}\lambda^2(T,B)/\delta_{nf}^2(B,T,\omega)} \right)^{1/2} \tag{1.3}$$

In terms of the complex microwave resistivity of the superconductor one writes $\widetilde{\rho} = \rho_1 + \mathrm{i}\rho_2 = \mathrm{i}\omega\mu_0\widetilde{\lambda}^2$ and, after some algebra, one gets:

$$\begin{aligned} \rho_1 &= \frac{1}{1+4(\lambda/\delta_{nf})^4}\left[r_1(B,T,\omega) + 2\left(\frac{\lambda}{\delta_{nf}}\right)^2 r_2(B,T,\omega) \right] \\ \rho_2 &= \frac{1}{1+4(\lambda/\delta_{nf})^4}\left[r_2(B,T,\omega) - 2\left(\frac{\lambda}{\delta_{nf}}\right)^2 r_1(B,T,\omega) \right] \end{aligned} \tag{1.4}$$

where $r_1 = \mathrm{Re}[\rho_v]$, $r_2 = \mathrm{Im}[\rho_v] + 2\rho_{nf}\left(\frac{\lambda}{\delta_{nf}}\right)^2$ and $\rho_{nf} = 1/\sigma_{nf}$.

Eqs.(1.4) contain in a selfconsistent way both the quasiparticle contribution (through λ and δ_{nf}) and the motion of vortices (through ρ_v). The model is founded on the interaction between charge carriers and a system of magnetic vortices moving under the influence of rf currents and pinning phenomena. Charge carriers are thought as bearing superconducting currents, represented by a superfluid characterized by the London penetration depth λ which gives rise to an imaginary conductivity $1/\mu_0\omega\lambda^2$, and normal currents represented by σ_{nf}. These equations should be considered as *master equations*, since the actual dependence of both ρ_1 and ρ_2 as a function of temperature, magnetic field and frequency is dictated by the functional dependence of λ, δ_{nf} and ρ_v with respect to the same parameters. In particular, λ and δ_{nf} (through σ_{nf}) may vary as a function of temperature and field in different ways depending, e.g., on the order parameter symmetry. On the other hand, ρ_v may depend on temperature, magnetic field and frequency in several different ways, depending on the pinning strength, inter-vortices interactions and periodicity of the pinning potential. This will in general result in rather different dependencies for both the real and the imaginary part of the resistivity.

In order to catch some general feature out of Eqs.(1.4), we first consider the vortex motion contribution in the specific case of frequencies not too small, so that the long range order of the pinning potential becomes irrelevant. This should be in general the case for microwave frequencies. In this case, one may use the specific expression of ρ_v obtained for periodic pinning potentials [88, 89]:

$$\begin{aligned}\mathrm{Re}[\rho_v] &= \rho_{ff}\frac{\epsilon+(\nu/\nu_0)^2}{1+(\nu/\nu_0)^2}\\ \mathrm{Im}[\rho_v] &= \rho_{ff}\frac{1-\epsilon}{1+(\nu/\nu_0)^2}\frac{\nu}{\nu_0}\end{aligned} \tag{1.5}$$

where ϵ is a creep factor that ranges from $\epsilon = 0$ (no flux creep) to $\epsilon = 1$ (free vortex motion), and ν_0 is a characteristic frequency which, in absence of creep phenomena, corresponds to the depinning frequency $\nu_p = \kappa_p/2\pi\eta$. It is worth to stress that, although Eqs.(1.5) have been obtained within a specific assumption, similar behaviors as a function of frequency can be reasonably assumed even in more general cases: for vortices interacting with pinning centers, in fact, it is always possible to define a characteristic frequency ν_0 which separates a low frequency regime, in which the vortices cannot follow the alternate Lorentz force acting on them, from a high frequency regime where vortices oscillate in-phase around their equilibrium positions even when strongly pinned. If the frequency is swept across ν_0, the observed $\mathrm{Re}\,[\rho_v]$ increases from a low frequency value to the free flow value, while $\mathrm{Im}\,[\rho_v]$ presents a maximum at ν_0. This is qualitatively the behavior predicted by Eqs.(1.5).

In addition, if it is further verified that $\omega\tau_{qp} \ll 1$, σ_{nf} is real and does

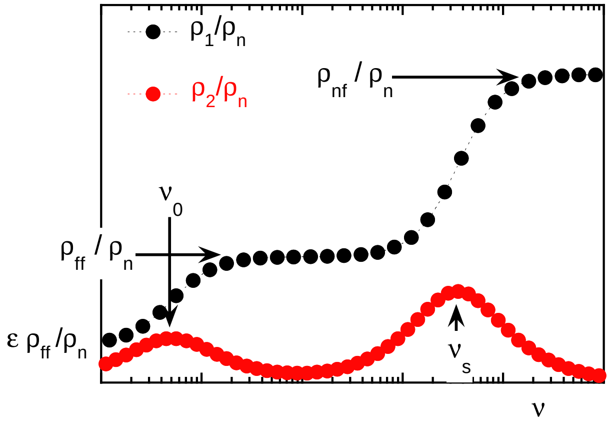

Figure 1.4: Exemplification of $\rho_1(\nu)$, $\rho_2(\nu)$ curves (frequency in a logarithmic scale) according to Eqs.(1.6). Also shown, the role of the main parameters.

not depend on frequency. One may write $2(\lambda/\delta_{nf})^2 = \nu/\nu_s$, with $\nu_s = 1/2\pi\mu_0\sigma_{nf}\lambda^2$. With these substitutions Eqs.(1.4) can be explicitly rewritten as follows:

$$\begin{aligned}\rho_1 &= \frac{1}{1+(\nu/\nu_s)^2}\left[\rho_{ff}\frac{\epsilon+(\nu/\nu_0)^2}{1+(\nu/\nu_0)^2}+\frac{\nu}{\nu_s}\left(\frac{\nu}{\nu_s\sigma_{nf}}+\rho_{ff}\frac{1-\epsilon}{1+(\nu/\nu_0)^2}\frac{\nu}{\nu_0}\right)\right] \\ \rho_2 &= \frac{1}{1+(\nu/\nu_s)^2}\left[\frac{\nu}{\nu_s\sigma_{nf}}+\rho_{ff}\frac{1-\epsilon}{1+(\nu/\nu_0)^2}\frac{\nu}{\nu_0}-\frac{\nu}{\nu_s}\left(\rho_{ff}\frac{\epsilon+(\nu/\nu_0)^2}{1+(\nu/\nu_0)^2}\right)\right]\end{aligned} \tag{1.6}$$

It is interesting to discuss some useful limits of Eqs.(1.6).

The conventional low temperature limit. At temperature low enough, so that creep phenomena are not relevant ($\epsilon = 0$ and $\nu_0 = \nu_p$) and the normal fluid conductivity can be neglected, one has $\sigma_{nf} \to 0$ and $\nu_s \to \infty$, so that

$$\begin{aligned}\rho_1 &= \rho_{ff}\frac{1}{1+(\nu_p/\nu)^2} \\ \rho_2 &= \mu_0\omega\lambda^2+\rho_{ff}\frac{\nu_p/\nu}{1+(\nu_p/\nu)^2}\end{aligned} \tag{1.7}$$

which are equivalent to the conventional Gittleman-Rosenblum expressions for the microwave resistivity in the mixed state, Eqs.(1.1), apart from the first term in the imaginary part, representing the zero-field imaginary conductivity.

The two-fluid limit. As a second example, it is easily seen that for $B \to 0$ one has $\rho_{ff} = 0$ and Eqs.(1.6) reduce to the two-fluid conductivity, Eqs.(1.2).

The high frequency limit: free flow. When the measuring frequency is much larger that the vortex characteristic frequency, $\nu \gg \nu_0$, Eq.(1.6) reduces to

$$\begin{aligned} \rho_1 &\simeq \frac{1}{1+(\nu/\nu_s)^2}\left[\rho_{ff}+\frac{1}{\sigma_{nf}}\left(\frac{\nu}{\nu_s}\right)^2\right] \\ \rho_2 &\simeq \frac{\nu/\nu_s}{1+(\nu/\nu_s)^2}\left(\frac{1}{\sigma_{nf}}-\rho_{ff}\right) \end{aligned} \tag{1.8}$$

In this limit vortices oscillate in phase making very short displacements from their equilibrium position. Despite the possibly finite pinning, as could be determined by, e.g., dc resistivity or magnetization, the vortex response coincides with the free flux flow. In this case the response depends on intrinsic physical quantities only: ν_s, ρ_{ff} and σ_{nf}. The analysis of the data in this limit is more stringent, since only three parameters are involved (and, in addition, ν_s and σ_{nf} are related one to each other). It should be noted that this limit might apply to various measurements at the high edge of the microwave spectrum.

Up to now we have mainly considered the vortex motion. However, both superfluid and quasiparticle densities are affected by the magnetic field. In fully gapped superconductors, such as conventional superconductors, the quasiparticle density of states (DOS) at Fermi level is nonzero only within the vortex core. As a consequence, the total DOS is proportional to the area occupied by the cores and the field-dependent depletion of the superfluid fractional density is simply $\Delta x_s \propto \frac{\xi^2}{R^2} \approx B/B_{c2}$, where the coherence length ξ gives the dimension of the vortex and $R \sim \sqrt{\Phi/B}$ is the intervortex spacing, with Φ the total magnetic flux through the sample.

The situation is rather different in superconductors with lines of nodes in the gap. In this case, it has been shown that extended states *outside* of the vortex core have the most relevant weight [95, 96]. However, such states have zero DOS only at the Fermi level, and any finite energy brings a variation of the quasiparticle fractional density. As an example, circulating supercurrents around vortices give rise to a Doppler shift [97, 95] of the quasiparticle energy. This results in a depletion of the superfluid fractional density which is proportional to the spatial range of the circulating supercurrents, $min\{\lambda, R\} \approx R$ for fields not too low, and to the number of vortices $\sim B/\Phi$. As a result, one has $\Delta x_s \approx \sqrt{B/B_{pb}}$ where B_{pb} is a characteristic pair-breaking field, that can depend on the gap gradient at the nodes, on impurity scattering and temperature, but it can be assumed (as a first approximation) to be $B_{pb} \approx cB_{c2}$ [96], with $c \sim o(1)$.

Thus, in general one can write:

$$x_s(T,B) = x_{s0}(T) - \Delta x_s(T,B) \approx x_{s0}(T)\left[1-\left(\frac{B}{cB_{c2}}\right)^{\alpha}\right] \tag{1.9}$$

where α depends on the symmetry of the gap and on impurities [98], and in clean cases $\alpha = 1$ or $\alpha = \frac{1}{2}$ in fully gapped superconductors and in superconductors with lines of nodes, respectively. More accurate treatments [99, 100] do not change the qualitative result of a significant reduction of the superfluid density with the application of a magnetic field.

It is useful to plot some illustrative curve of the theoretical predictions, in order to elucidate the role of the different parameters. We will also make use of the limits above discussed.

We present first schematic shapes of the curves $\rho_1(\nu)$ and $\rho_2(\nu)$ as obtained from the general expression, Eqs.(1.6). We stress that when plotting resistivity vs. frequency it is not necessary to assume any specific temperature or field dependence for the quantities appearing in the equations. As shown in Fig.(1.4), the shape of the two curves $\rho_1(\nu)$ and $\rho_2(\nu)$ is affected in different ways by the various parameters (ρ_{ff}, ϵ and ν_0 determine the vortex motion, σ_{nf} and ν_s the properties of the quasiparticles). In particular, it is seen that even a rather simple model can give significantly different curves for $\rho_1(\nu)$ and $\rho_2(\nu)$. Since the variation range of the involved parameters is very wide[2], it is evident that a wide measuring frequency range can prove especially useful in the interpretation of the data.

In this Chapter we will report also data for the complex resistivity at a single frequency (resonant cavity technique) and as a function of the field, so that it is appropriate to present and discuss some theoretical curve at a fixed frequency. In order to plot the microwave resistivity *vs.* the magnetic field, it is necessary to make some additional hypotheses with respect to the frequency plots. In particular, it is necessary to assume the field dependence of the parameters defining the frequency dependence of the resistivity. In order to limit the number of the assumptions, we restrict ourselves to the case of sufficiently high frequency ($\nu \gg \nu_0$) so that the field variations of ν_0 (and, to a larger extent, of ϵ) become almost irrelevant. We also assume that the vortex viscosity η does not depend on field. For the quasiparticle and superfluid response, we assume that $\sigma_{nf} = x_n(T,B)\sigma_n$ and $\lambda^2 = \lambda_0^2/x_s(T,B)$, with x_n being the normal fractional density, related to x_s through the relation $x_n + x_s = 1$. We momentarily neglect in this illustrative case possible

---

[2] All these parameters are expected to vary as a function of temperature and magnetic field. In particular, $\nu_s \to 0$ and $\sigma_{nf} \to \sigma_n$ as the superconductor enters the normal state by increasing the field or temperature; for fields not too low, $\rho_{ff} \sim B$; $\epsilon \sim 0$ at low temperatures and $\epsilon \to 1$ at higher T. Finally, the behavior of ν_0 might be extremely dependent on the pinning characteristics of the specific sample.

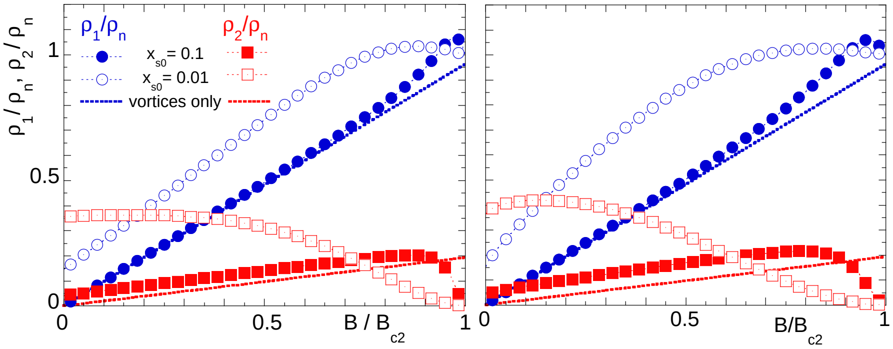

Figure 1.5: Reduced field dependence of the vortex state complex resistivity according to the CC model [88], Eq.(1.4), for $\nu/\nu_0 = 5$. The curves for small (full symbols) and very small (open symbols) superfluid concentration are reported, and compared to the vortex motion contribution alone (Re$[\rho_v]$, Im$[\rho_v]$ as in Eq.(1.5), dashed lines). Parameters are reported in the text. Left panel, fully gapped superconductors. Right panel, superconductor with lines of nodes in the gap (see text).

differences between the scattering times of quasiparticles and normal electrons. We plot the calculated curves at the fixed frequency $\nu = 50$ GHz as a function of the reduced applied magnetic field in two cases: fully gapped superconductor and superconductor with lines of nodes in the gap, in the left and right panels of Fig.1.5, respectively. Curves are plotted for different values of the zero field superfluid density x_{s0} (which is equivalent to different temperatures). We use typical values for high T_c superconductors, $\lambda_0 = 1000$ Å and $\sigma_n = 10^6$ S·m^{-1}. We also fix $\nu_0 = 10$ GHz as reported for HTCS at low temperature [34, 43, 134] and $\epsilon = 0$, both independent on field. In both cases at relatively large superfluid concentration ($x_{s0} = 0.1$) the real part of the resistivity is substantially coincident with Re$[\rho_v]$ at low fields (ρ_v is the resistivity due to the vortex motion, and it does not depend, by definition, on the superfluid density x_s). This is due to the fact that with the values used for λ_0 and σ_n, $\nu_s \gg 50$ GHz at low temperatures and fields, so that, as discussed previously, Eqs.(1.6) reduce to the Gittleman-Rosenblum expression, Eq.(1.1). However, this is no longer the case at very small superfluid density (i.e., at higher temperatures close to T_c or with strong pair breaking), $x_{s0} = 0.01$, where neglecting the quasiparticle contribution results in a rather large error. Interestingly, as reported in Fig.1.6, in the case of lines of nodes in the superconducting gap, at low fields the variation of the imaginary part of the resistivity is clearly found to increase as $\sim \sqrt{B}$ even in presence of flux flow (linear in the applied field), while for fully gapped superconductors this increase turns out to be linear with B. Moreover, a

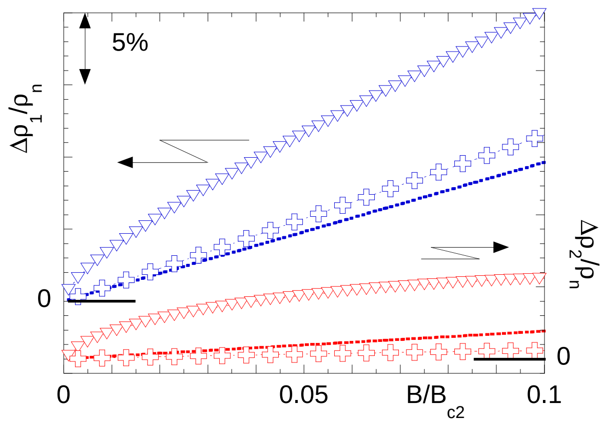

Figure 1.6: Plot of the field variation of the complex resistivity, at low reduced fields. Parameters as in Fig.1.5, with $x_{s0} = 0.01$. Blue symbols, left scale: $\Delta\rho_1/\rho_n = \left[\rho_1(B) - \rho_1(0)\right]/\rho_n$. Red symbols, right scale: $\Delta\rho_2/\rho_n = \left[\rho_2(B) - \rho_2(0)\right]/\rho_n$. Dotted lines, vortex motion only. Crosses, fully gapped superconductor. Triangles, superconductor with lines of nodes in the gap. A sublinear field dependence is clear when the superconducting gap has lines of nodes.

closer inspection of the $\rho_1(B)$ curve shows that a partial $\sqrt{B}$ dependence is also present in the real part of the resistivity, for superconductors with lines of nodes in the gap, at sufficiently low superfluid concentration. It is important to stress that the role of quasiparticles is relevant whenever ν_s is not much larger than the measuring frequency ν. Due to the parameters used, in the case above exemplified ν_s is always much larger that ν (50 GHz) unless $x_s \to 0$, that is for $T \simeq T_c$ (or $B \simeq B_{c2}$).

Before commenting experimental results concerning different superconductors, we now briefly discuss which are the main possible differences between the relatively simple scenario depicted up to now and the real world. First of all, we have neglected any creep phenomena for vortices ($\epsilon = 0$), which is unlikely to be correct at high temperatures. A non-vanishing ϵ will strongly influence the low frequency ($\nu \lesssim \nu_0$) resistivity. More important, since $\nu_0 = \kappa_p/2\pi\eta$ only for $\epsilon = 0$, an increasing ϵ could introduce rather strong temperature and/or field dependencies in ν_0. In particular, since ν_0 is expected to grow rather fast with increasing ϵ, in a measurement at fixed frequency one might have $\nu > \nu_0$ at low temperatures or fields and $\nu < \nu_0$ at higher temperatures or fields. This will result in unpredictable shapes for the curves $\rho(H)$ or $\rho(T)$, depending on the field/temperature variation of ν_0.

The second main hypothesis which is not necessarily verified concerns the quasiparticle conductivity. Smaller values of ν_s can substantially change the quasiparticle contribution to the resistivity. As an example, quasiparticle relaxation rates shorter than the normal state values, as reported by several authors [64, 65, 66], would tend to decrease substantially ν_s. One might have as a consequence large quasiparticle contributions even at low temperatures and fields.

Finally, it must be noticed that Eqs.1.5 for the vortex resistivity are obtained in the rather special case of periodic pinning potential. Moreover, they do not take into account the resistivity due to Josephson or Abrikosov-Josephson vortices, whose dynamics might be rather different with respect to standard vortices. The expression for the vortex resistivity ρ_v might then be rather different, in the most general case. However, we will show in the following that most of the main features observed in the microwave data of several superconducting materials can be quantitatively explained using the theoretical expressions cited up to now. We will come back to specific points during the discussion of the data in Sec.1.4

1.3 EXPERIMENTAL SECTION

1.3.1 Samples

All measurements here presented were performed in thin, high-quality superconducting films. $YBa_2Cu_3O_{7-\delta}$, $SmBa_2Cu_3O_{7-\delta}$, and MgB_2 were investigated extensively. Samples were squares, of side l and thickness d. Substrates have been carefully chosen for microwave measurements. The crystal structure was investigated by X-ray $\Theta - 2\Theta$ diffraction. The c-axis orientation was assessed by measuring the full-width-half-maximum (FWHM) of the rocking curve of an appropriate peak. In-plane X-ray $\Phi-$scan was measured in samples Y1, Y2, Y3, Sm1, Sm2, and M1, showing excellent in-plane epitaxiality. Surface roughness was investigated by AFM over typical 1 μm $\times$ 1 μm area. All cuprates sample were nearly optimally doped or slightly overdoped. T_c and the resistivity above T_c, ρ_0, were estimated by electrical transport methods. Depending on the sample, we used *dc* or microwave resistivity. In this latter case T_c was estimated from the inflection point of the temperature-dependent real part of the microwave resistivity (this temperature is found to coincide with the temperature where the real and imaginary parts of the microwave fluctuational conductivity equal one to the other, which is an accurate evaluation of the mean-field critical temperature [101]), and ρ_0 from the measured real part ρ_1 in zero magnetic field. Typical ± 0.5 K uncertainties of these methods are inessential for the purposes of the present paper. Material parameters and appropriate references are reported in Table 1.1. More details on sample preparation and characterization are

Material	YBCO	YBCO	YBCO	YBCO	SmBCO	SmBCO	MgB_2
Sample no.	Y1	Y2	Y3	Y4	Sm1	Sm2	M1
Substrate	$LaAlO_3$	$LaAlO_3$	$LaAlO_3$	CeO_2/YSZ	$LaAlO_3$	$LaAlO_3$	sapphire
Thickness (nm)	220	220	220	200	220	220	100
Lateral dimension (mm)	10	10	10	10	10	10	5
$\Theta - 2\Theta$ FWHM	0.1°	0.1°	0.1°	0.2°	0.2°	0.2°	N.A.
Surface roughness (nm)	2	2	2	N.A.	3	3	N.A.
T_c (K)	89.5	89.5	90	88	87	87	36
ρ_0 ($\mu\Omega$·cm)	130	140	130	250	300	300	5
References	[102, 103]	[102, 103]	[102, 103]	[104]	[105, 106]	[105, 106]	[107]

Table 1.1: Data for the structural and electrical characterization of the samples investigated. $\rho_0 = \rho_1(100\text{ K}, 48\text{ GHz})$ and $\rho_{dc}(40\text{ K})$ in RE-BCO and MgB_2, respectively. N.A.: not available.

reported in the References (see Table).

1.3.2 Microwave response in thin films.

Since in all the measured samples the thickness is of the order of, or smaller than, the commonly reported values for the penetration depth, it is appropriate to shortly describe the electromagnetic response of an electromagnetically thin (super)conducting film.

In the case of bulk samples, for which the sample thickness is much greater than the electromagnetic field penetration depth (of the order of $\min(\lambda, \delta_{nf})$), the surface impedance is given by the usual expression already mentioned: $Z_s = (\mathrm{i}\omega\mu_0\tilde{\rho})^{1/2}$.

When the sample thickness $d \lesssim \min(\lambda, \delta_{nf})$, the electromagnetic field is transmitted through the film and reaches the substrate and any supporting layer, usually a metallic backplate. The field is therefore determined by the interaction with both the underlying layers and the film of finite thickness. In this situation the simple expression for Z_s no longer holds, being substituted by an effective surface impedance Z_s^{eff} which can be derived by means of standard impedance transformation relations [108]:

$$Z_s^{eff} = Z_s \frac{Z_d^{eff} + \mathrm{i}Z_s \tan(k_s d)}{Z_s + \mathrm{i}Z_d^{eff} \tan(k_s d)} \tag{1.10}$$

where $k_s = \mu_0\omega/Z_s$ is the HTCS propagation constant and Z_d^{eff} is the effective surface impedance of the substrate. The full expression of Eq.(1.10) can be significantly simplified when two main conditions are met: $|Z_d^{eff}| \gg |Z_s|$, meaning that the substrate contribution can be neglected, and $d \ll \min(\lambda, \delta)$, which is usually the case for epitaxially grown high T_c superconductor films. In this case the so-called thin-film approximation [109, 110] is obtained:

$$Z_s^{eff} \simeq \frac{\tilde{\rho}}{d} \tag{1.11}$$

The applicability of this equation heavily depends on the (possibly temperature-dependent) properties of the substrate. Metallic [111] and semiconducting [112, 113] substrates strongly affect Z_s^{eff} and they impose the use of the full expression, Eq.(1.10). On the other hand dielectric substrates with backing metallic plate have often impedances high enough so that Eq.(1.11) can safely be used[3].

1.3.3 Cavity measurements.

The microwave response at high frequency was measured in RE-BCO by the end-wall cavity technique [118] at 48.2 GHz. The cylindrical cavity, of 8.2 mm diameter, was inserted in a liquid/solid Nitrogen cryostat, so that temperatures in the range 60-150 K could be reached. Cryogenic waveguides were used in order to couple the one-port cavity to the external microwave source. The temperature of the entire cavity, including the sample, could be stabilized for hours within ±10 mK. A magnetic field H was applied along the c axis and supplied by a conventional electromagnet. The maximum attainable field in this setup was $\mu_0 H \leq 0.8$ T. In the following, we will assume that inside the sample $B \simeq \mu_0 H$ [4].

For the measurements, undercoupling of the cavity and the TE_{011} resonant mode were chosen. In this mode the currents flow along circular paths on the end-wall occupied by the sample, have zeroes at the center of the end walls and at the joints between the end walls and the body of the cavity, and maxima at half the radius of the end wall. This configuration allows to neglect the losses due to imperfect electric contact between the sample and the cavity; moreover, it makes possible the use of a mechanical stub to tune the cavity at the desired resonant frequency (in our case, in the range 48.0 ± 0.5 GHz). The degenerate TM mode, strongly suppressed by electrical isolation between the end walls and the body of the cavity, was further shifted in frequency by appropriate mode traps. Fig.1.7 reports a sketch of the cavity setup and of the pattern of the currents on a typical 10 mm × 10 mm sample.

Measurements of the field and/or temperature induced changes of the quality factor Q and resonance frequency f_0 yielded changes in the effective surface impedance through the well known expression $\Delta Z_s^{eff}(H,T) = G\Delta\left[\frac{1}{Q(H,T)} - 2\mathrm{i}f_0(H,T)\right]$, where G is an appropriate geometrical factor

---

[3] Noticeable exceptions are dielectrics with strong temperature dependent permittivity [110, 114, 115, 116] or with an accidentally unfavorable combination of thickness, permittivity and operating frequency [117].

[4] We note that demagnetization effects determine a penetration field much smaller than H_{c1} in thin films [119], and field inhomogeneities inside the sample are expected (and also directly found [120]) to be irrelevant in thin films for fields greater than a few mT in our temperature range.

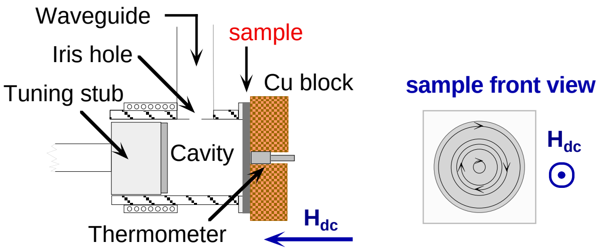

Figure 1.7: Left: straight section of the resonant cavity. Right: current patterns on the square sample.

[108]. Separate calibration of the response of the cavity allowed for the determination of the absolute value of R_s^{eff}. In most of the measurements here reported, Q and f_0 were measured as a function of the magnetic field at various fixed temperatures in the range 60 K - T_c. Measurements were performed by sweeping the field from zero up to 0.8 T either after zero-field-cooling (ZFC) to the desired temperature, or by increasing the temperature after each field sweep. We did not observe hysteresis, apart a 10% effect at temperatures below 70 K in some of the samples. In some cases, to check the relevance of the hysteresis, full magnetic cycles were performed. Measurements here reported refer only to the cases where hysteresis is absent, or well below 10% of the total response.

From the field induced change of Q and f_0 the field induced change of the effective surface impedance $\Delta Z_s^{eff} = Z_s^{eff}(H,T) - Z_s^{eff}(0,T)$ could be obtained [121]. Due to the small thickness of the films, one has $Z_s^{eff} = \tilde{\rho}/d = \rho_1/d + \mathrm{i}\rho_2/d$, where $\tilde{\rho}$ is the complex resistivity.

The main experimental errors are due to the following reasons: the absolute value of Z_s^{eff} is affected by errors in the calibration of the cavity and in the evaluation of the geometrical factors [122, 123, 124]. Additionally, $\tilde{\rho}$ has an intrinsic uncertainty due to the evaluation of the film thickness (typically 10%). By contrast, calibration of the cavity does not affect the field variation of $\tilde{\rho}$ at fixed temperature, and geometrical factors and film thickness give only a possible overall scale factor. All these sources of errors are strongly reduced (if not eliminated at all) when working with reduced complex resistivity changes, $\Delta\tilde{\rho}/\rho_0 = \Delta\rho_1/\rho_0 + \mathrm{i}\Delta\rho_2/\rho_0$, with $\rho_0 = \rho(100$ K) in YBCO and SmBCO. In the following the data will be reported in one of the mentioned formats.

Finally, some useful features of the present setup should be stressed. First, the microwave currents and fields lie in the (a,b) planes, thus avoiding any c axis contribution to the measured response. Second, the dc magnetic field is perpendicular to the microwave currents (maximum Lorentz force

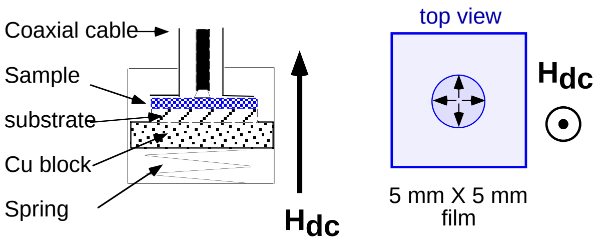

Figure 1.8: Left: straight section of the Corbino disk cell. Right: current patterns on the square sample.

configuration). Third, the microwave currents essentially probe only an annular region of 4.1 mm mean diameter and ∼ 2 mm width, centered on the sample. For the subsequent discussion, it is relevant that flux lines are not forced to cross the border of the sample: the oscillation induced by the microwave currents are limited to the annular region above mentioned. In particular, no edge effects are relevant in our configuration.

1.3.4 Corbino disk measurements.

The frequency dependence of the vortex-state microwave response was measured in YBCO and MgB_2 films. Measurements are obtained through a Corbino disk geometry [34]: a swept frequency microwave radiation is generated by a vector network analyzer (VNA) and guided to the sample under study through a coaxial cable. The sample, placed inside the cryomagnetic apparatus, shortcircuits the coaxial cable. A double spring is used to obtain a good electrical contact between the end cable connector and the sample. To further improve the contact, a thin annular indium foil is placed between the sample and the external part of the coaxial cable. Due to the limitations discussed below, data are reported for the frequency range 2-20 GHz, well inside the capabilities of the VNA (45 MHz-50 GHz) and of the cables (cut-off frequency 50 GHz). A magnetic field up to 10 T was applied along the c axis. The temperature ranges 70 K - 100 K and 5 K - 40 K were explored, in YBCO and MgB_2, respectively. In Fig.1.8 we show a sketch of the Corbino disk cell and of the current pattern on the sample.

In principle, a measurement of the complex reflection coefficient Γ_0 at the sample surface directly yields the complex effective surface impedance Z_{eff} of the sample by the standard relation

$$\Gamma_0 = \frac{Z_s^{eff} - Z_0}{Z_s^{eff} + Z_0}$$

where Z_0 is the impedance of the cable [108]. In our case, however, the measured quantity is the reflection coefficient at the instrument location Γ_m, which contains, besides the response of the sample, reflections and attenuation due to the cable line between the sample and the VNA. Due to the long line, necessary to place the VNA far from the stray field of the magnet, the contribution of the sample to the overall Γ_m is rather small. Further, the response of the part of the line inside the cryostat depends on the temperature profile across the cable, that varies in general during the measurement. Thus, full calibration of the cable and, consequently, direct measurements of absolute values of the impedance of the sample are not feasible. To overcome this problem, we developed a custom calibration procedure, through which we could obtain the variations of the effective surface impedance with the temperature or with the field, $\Delta Z_s^{eff}(\nu, H, T)$. The description of the calibration procedure is rather cumbersome, and it has been extensively described elsewhere [125, 126]. Here we recall only the major hypotheses necessary to obtain the impedance data from the measured complex reflection coefficient.

Reliable measurements of the *temperature* variations of the effective surface impedance, $\Delta Z_s^{eff}(\nu, H, T) = Z_s^{eff}(\nu, H, T) - Z_s^{eff}(\nu, H, T_{ref})$, require *(i)* that the temperature variation of the complex reflection coefficient are not dominated by the change in the response of the cable, and *(ii)* that at least at sufficiently low temperature $\Gamma_0(\nu) \simeq -1$ (or, equivalently, $R_s^{eff}, X_s^{eff} \ll Z_0$) [125]. In particular, variations of R_s^{eff} mainly reflect on variations in the modulus of Γ_0, while variations of X_s^{eff} have as a main effect a phase change of Γ_0. The accuracy and reliability of the measurement of ΔR_s^{eff} and ΔX_s^{eff} depend then on relative variations of modulus and phase of Γ_0 with respect to corresponding variations (due to, e.g., the change of the cable characteristics) of Γ_m, respectively. It turns out that for the measurements of R_s^{eff} the requirements are fulfilled in the temperature ranges 5 K - 40 K and 70 K - 100 K in MgB_2 and YBCO, respectively. Unfortunately, the temperature variations of the phase signal due to the sample are of the same order of magnitude of the temperature variations of the phase due to the cable, so that a reliable measurement of X_s^{eff} is not feasible with this kind of measurement. No such problems arise at fixed temperature and with sweeping field: in this case, the response of the cable is almost exactly constant (we checked that the line has a very small magnetic response): *field* variations $\Delta Z_s^{eff}(\nu, H, T_0) = Z_s^{eff}(\nu, H, T_0) - Z_s^{eff}(\nu, 0, T_0)$ can be reliably obtained.

These measurements can be converted to absolute values of R_s^{eff} and/or X_s^{eff} by assuming some known $R_s^{eff}(\nu)$ or $X_s^{eff}(\nu)$ at some specific temperature or field. In general, one can take $R_s^{eff}(\nu) \simeq 0$ at sufficiently low temperatures and fields, while X_s^{eff} can be obtained from normal state measurements (at high enough temperatures or fields).

There are a few additional remark on the different behavior of the two materials investigated with the Corbino disk. First, the quality of the electrical contact between the coaxial connector and the film is much better in MgB_2 than in YBCO. This results in reliable measurements in the ranges 2 - 20 GHz and 5 - 20 Ghz in MgB_2 and YBCO, respectively. Second, with the available magnetic field it was possible to reach the normal state in MgB_2, so that absolute measurements of R_s^{eff} and X_s^{eff} can be obtained by increasing the field above the upper critical field. In YBCO measurements were taken with field-cooling the sample (thus lowering the temperature), and only the real part of Z_s^{eff} could be obtained. Finally, even after the calibration procedure, there still remain detectable oscillations in the frequency-sweeps. Those oscillations, together with uncertainties in geometrical factors, are eliminated by reporting the data normalized to the values measured above T_c.

As for the cavity measurements, the thin film approximation holds [110] and one has $Z_{eff} = \widetilde{\rho}/d$. Most important, like and more than in the cavity measurements, in the Corbino disk geometry there are no contributions at all from vortex entry or exit: the area probed by the microwave currents is a small circle, of radius ∼2 mm, at the center of the sample, and currents flow along linear paths between the inner contact and the outer conductor, so that vortices are forced to oscillate along circular orbits. Again, no edge effects affect our measurements.

1.4 RESULTS

In this Section, we present and discuss the results obtained on the various superconducting materials under study. We present separately the results for the different materials.

1.4.1 $YBa_2Cu_3O_{7-\delta}$

$YBa_2Cu_3O_{7-\delta}$ is a somewhat paradigmatic case: as it will be shown in the following, the microwave properties in the vortex state follow quite closely the simple models summarized in Sec.1.2, allowing for a rather detailed discussion of the various dynamical regimes as a function of frequency, temperature and magnetic field. By means of combined wideband (5-20 GHz) and high-frequency (48 GHz) measurements we will show (a) that it exists a relatively wide temperature range below the critical temperature T_c in which the resistivity, while clearly lower than the normal state value, is at the same time independent on frequency, indicating that the effect of pinning (if any) is not relevant in this T range, (b) that vortex motion follows closely the predictions of the mean-field, Coffey-Clem theory, and (c) that approaching

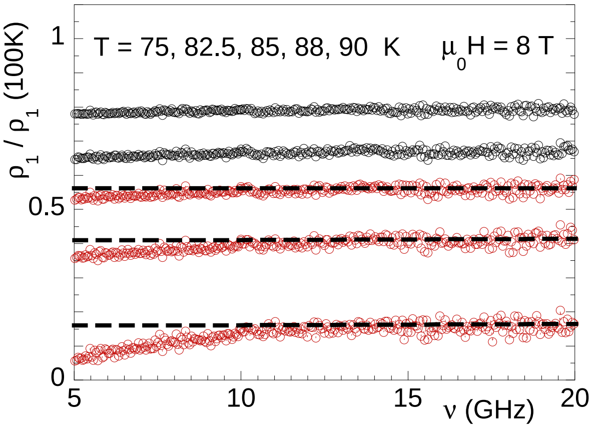

Figure 1.9: Normalized real resistivity in YBCO vs. frequency at various temperatures and $\mu_o H = 8$ T. A detectable frequency dependence only appears for T <85 K (red data curves). Temperature increases from bottom to top.

the critical temperature the field dependence of the microwave resistivity points to a relevant role of the field-dependent superfluid depletion. We also obtain the temperature dependence of the vortex parameters η and ν_0.

We begin with the frequency dependence of the microwave real resistivity ρ_1 measured in sample Y3. In Fig.1.9 we report the frequency dependence of ρ_1/ρ_0 measured with the Corbino disk at various temperatures and at a fixed field $\mu_0 H$= 8 T. As it can be seen, while ρ_1 is sensibly lower than ρ_0 for $T < 90$ K, a frequency dependence is observed only below $T = 85$ K< T_c. This is a first indication that in the superconducting state there is a region of the (H, T) phase diagram where the microwave response in the frequency region here investigated is independent (or very weakly dependent) on frequency. This finding restricts the range of physical phenomena that can give rise to the measured response. More insight can be gained by representing the data at fixed frequency as a function of the temperature, as depicted in Fig.1.10, where we compare the normalized real resistivity at two fixed frequencies (6 and 20 GHz) as a function of temperature, for $\mu_0 H = 2$ T and 8 T. At each field the data at two different frequencies lie on a single curve in a temperature range extending from above to below T_c, while they are markedly different at lower temperatures, below an easily estimated crossover temperature $T_f(H)$. This abrupt change in the frequency dependence across T_f marks the boundary between two different dynamic regimes.

The nature of these two regimes can be understood considering the interplay of vortex and quasiparticle response: at low temperature flux motion

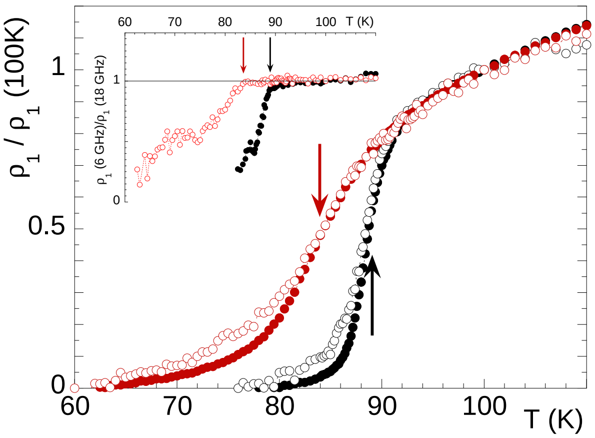

Figure 1.10: Normalized real resistivity in YBCO vs. temperature at 6 GHz (full symbols) and 20 GHz (open symbols) and $\mu_o H = 2$ T (black symbols) and 8 T (red symbols). It is apparent that at each field there is no frequency dependence down to a typical temperature $T_f < T_c$, depicted by the arrows. The same feature is more evident in the inset, where the ratios $\rho_1(6\,\mathrm{GHz}, H, T)/\rho_1(20\,\mathrm{GHz}, H, T)$ have a clear departure from 1 at $T_f(H)$.

contribution is dominant. Near the transition temperature T_c quasiparticles play a significant role in the electromagnetic response (see Fig. 1.5). Very close and above T_c thermal fluctuations set in. In absence of disorder, all those mechanisms merge smoothly one into the other: in fact, the low temperature limit of the fluctuations-dominated dc resistivity coincides with the free flux flow [127], and a nearly frequency-independent ρ_1 results for both the fluctuation induced dissipation [128, 129, 130, 131, 132, 133] and for flux (free) flow resistivity (as can be easily seen from Eqs.(1.5), considering that the free flow limit corresponds to the case $\epsilon = 1$).

This framework drastically changes in presence of disorder. In that case vortices are more or less pinned to defects, and the overall dc resistivity becomes smaller than the free flow expression (viscous/plastic regime), eventually reaching a zero value if the interactions are strong enough to completely lock the flux lines (frozen regime). For what concerns the frequency response, the viscous/plastic as well as the frozen regime are characterized by a value of the creep factor ϵ (see Eqs.(1.5)) lower than unity (zero in the frozen regime), thus resulting in a frequency dependent real resistivity. In particular, Re$[\rho_v]$ should grow from ρ_{dc} to the free flow value ρ_{ff} when the frequency increases across the depinning frequency ν_p. This pinning frequency is estimated to be $\nu_p \simeq 10$ GHz [34, 43, 134] in YBCO, well within the frequency range here explored. As a result, the large frequency

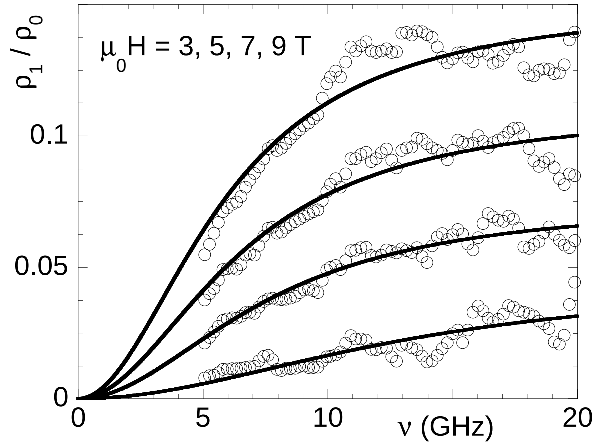

Figure 1.11: Typical swept-frequency measurements at different fields and $T = 70$ K. A marked frequency dependence is observed, denoting the change of vortex response. Continuous curves are fits with Eq.(1.5).

dependence of our data below T_f is explained with the increased effect of disorder. We now turn to the analysis of the data deep in the strongly frequency-dependent regime, that is $T < T_f$. We report in Fig.1.11 typical frequency sweeps for the normalized real resistivity in sample Y3 at low temperature and at various magnetic fields. It is immediately apparent that Re$[\rho_1]$ increases as a function of frequency, eventually reaching a saturation value at high frequencies. This is exactly the behavior expected from mean-field theories of the vortex state at sufficiently low temperatures. Within this framework, the field variation of the real resistivity is entirely given by the vortex motion, so that we fitted the data with the first of Eq.(1.5), using ϵ, ν_0 and $\rho_{ff}/\rho_n = \Phi_0 B/\eta\rho_n$ as fitting parameters. As it can be seen (thick lines), good fits are obtained. Similar results are obtained at different temperatures and fields. It should be mentioned that at low fields, and/or at high enough temperatures, the experimental curves become nearly featureless, and fitting is less reliable. We report here the vortex parameters obtained in the most reliable temperature and field ranges, that correspond to the region close to the frozen regime ($\epsilon \simeq 0$, $\nu_0 \simeq \nu_p$). It is found that ν_p smoothly depends on temperature and magnetic field, as reported in Fig.(1.12), and decreases for both increasing field and temperature.

The vortex viscosity, as obtained from swept frequency measurements in the low temperature region is reported in Fig.(1.13). It is remarkable that no significant magnetic field dependence is detected, thus indicating that the flux flow follows a magnetic-field linear dependence, $\rho_{ff} \sim B$.

To gain more insight in the electromagnetic response at microwave fre-

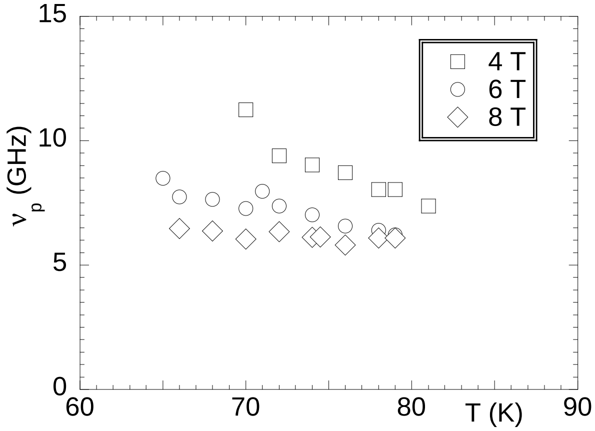

Figure 1.12: Temperature dependence at various fields of the depinning frequency ν_p in the temperature region below T_f. It is seen that $\nu_p < 15$ GHz, at all fields and temperatures.

quencies, we present now measurements of the complex resistivity obtained with the cavity resonator at a much higher frequency, $\nu = \omega/2\pi = 48$ GHz, as a function of the applied magnetic field on YBCO samples from the same batch. Measurements span the temperature range 65 K $-T_c$, and the field is limited to 0.8 T. In Fig.(1.14) we show typical field-sweeps of the variation of the complex resistivity at some significant temperature. It is seen that the real resistivity ρ_1 has an almost linear variation with the applied field, apart possibly the low field region, and that this linear dependence changes to a concave downward behavior approaching closely T_c. At the same time, the variation of the imaginary part $\Delta\rho_2$ with the field is nearly absent at low temperatures, and is *negative* at higher temperatures, close to T_c.

This behavior is easily recognized as an essentially free flux flow, with a possibly significant contribution of the field-induced superfluid depletion at high temperatures. This is completely consistent with the results from Corbino disk measurements, if one considers that ν_0 was found (at low temperature) below 15 GHz. As a consequence $(\nu/\nu_0)^2 \gg 1$ and, following Eq.(1.5), the vortex contribution reduces, as a first approximation, to the real flux flow term. Then, not too close to T_c, where the field dependence is essentially linear, $\rho_1 \simeq \rho_{ff} = \Phi_0 B/\eta$ and $\rho_2 \simeq 0$, from which the vortex viscosity is readily obtained. Such data points are reported in Fig.(1.13) and compared to the Corbino disk results. The agreement is excellent: field sweeps and frequency sweeps give exactly the same vortex viscosity.

At higher temperatures both the downward curvature of $\Delta\rho_1(H)$ and the pronounced, negative $\Delta\rho_2(H)$ can be accounted for by the field depen-

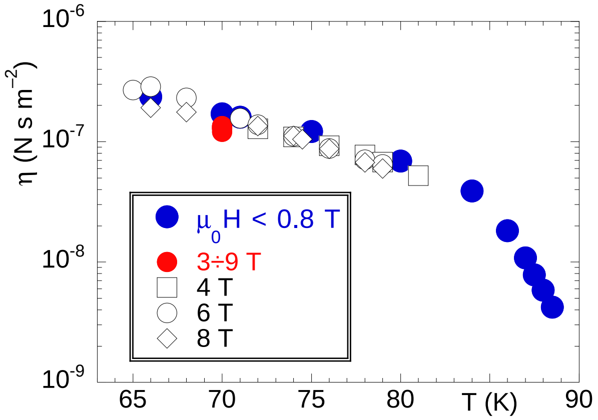

Figure 1.13: Temperature dependence of the vortex viscosity η in YBCO, obtained from Corbino disk swept frequency method (open symbols and red full dots, fields depicted in the figure) and from field-sweeps, resonant cavity technique (blue full dots). All the sets of data coincide, indicating that the intrinsic viscosity is measured. Moreover, no significant magnetic field dependence is detected.

dence of the superfluid and quasiparticle concentration. As discussed in Sec.1.2, in this case one has to use the full expression of the vortex state resistivity, Eq.(1.4), with the noticeable simplification that $\tilde{\rho}_v \simeq \rho_{ff}$ due to the high operating frequency. Fitting necessarily add other parameters: the zero field, temperature-dependent superfluid fraction $x_{s0}(T)$, the zero-temperature London penetration depth λ_0, the exponent α and the factor c (See Eq.(1.9)). The upper critical field is not a different fitting parameter, assuming $\eta = \Phi_0 B_{c2}/\rho_n$. We were not able to fit the pairs of curves $\Delta\rho_1(B)$, $\Delta\rho_2(B)$ with the exponent α=1 typical of fully-gapped wavefunction. Instead, by using $\alpha = \frac{1}{2}$ typical of a wavefunction with lines of nodes in the gap [46, 95, 96], we obtained fits as reported in Fig.(1.15) with the reasonable choice λ_0= 160 nm, and $c \simeq 0.15$ (we found $c \simeq 1$ in a different sample, with the analysis of the real part only [42]). The resulting η connects smoothly to the experimental data obtained at lower temperatures, and $x_{s0}(T) \sim \left[1 - \left(\frac{T}{T_c}\right)^2\right]$. While this is not a direct evidence for unconventional superconducting gap, we note that by taking into account the possible existence of lines of nodes (and the consequent increased weakness of the superfluid stiffness), the vortex state microwave response is fully described in its temperature, frequency and field dependence from well below up to very close to T_c. It is interesting to notice that the small quasiparticle contribution observed (apart very close to T_c) is consistent with $\tau_{qp} \sim \tau_n$

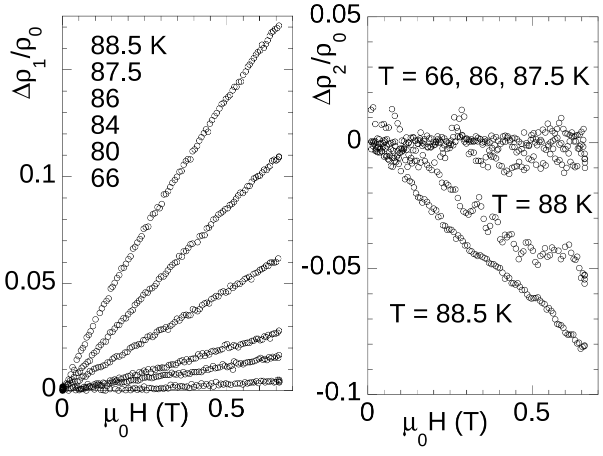

Figure 1.14: Typical magnetic field dependence of the variation of the complex resistivity in YBCO, measured at 48 GHz. Left panel, real resitivity. Right panel, imaginary resistivity. Note at high temperature the downward curvature in $\Delta\rho_1(H)$, and the decrease of $\Delta\rho_2(H)$.

(see Fig.1.5). Our results suggests then that in our YBCO films $\tau_{qp}/\tau_n \simeq 1$, closer to the results of [67] rather than to those of [65]. In this case YBCO is a paradigmatic case, and the simplest to understand. We will see in the following that all the other materials below reported present additional physics, that prevent from a straightforward application of the CC model. Additional mechanisms are revealed by measurements of the microwave response.

1.4.2 MgB$_2$

It is somehow expected that MgB$_2$, due to its firmly established two-gap nature, can hardly be described by oversimplified models. In order to didactically describe the difficulties hidden in the analysis of the data in this two-gap compound, we first present in Fig.(1.16) the real resistivity as a function of the frequency at fixed temperature and various magnetic fields, in complete analogy with the data for YBCO reported in Fig.(1.9). The reported data are qualitatively similar to those measured on YBCO, showing at each field a (real) resistivity increasing as a function of frequency, reaching a plateau value ρ_{pl} at high frequencies. Moreover, it is shown that, rather surprisingly, the simple, single-gap CC model quantitatively fit the data. One might then be led to the conclusion that simple vortex motion, as given by Eq.(1.5), captures the physics involved in microwave response in MgB$_2$. However, despite the quality of the fits, the behavior of the param-

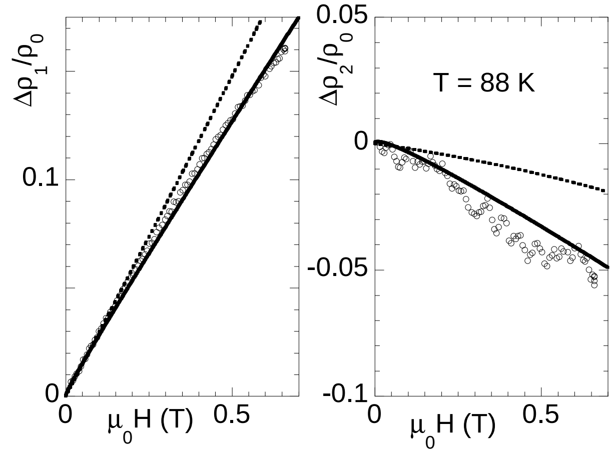

Figure 1.15: Typical fits of the magnetic field dependence of the variation of the complex resistivity in YBCO, measured at 48 GHz, with the flow expression, Eq.(1.8). Continuous lines: superconductor with lines of nodes, dashed lines: fully gapped superconductor.

eters is not easily understood within simple models for vortex motion: as an example, we report in Fig.(1.17) the ratio $\Phi_0 B/\rho_{ff,fit}$ that should coincide, in this oversimplified model, to the vortex viscosity η. It is found that $\Phi_0 B/\rho_{ff,fit}$ depends very strongly on the applied field (as opposed to the behavior theoretically expected and experimentally found in YBCO), while its temperature dependence changes with the field, becoming less and less temperature dependent as the field increases. More puzzling results can be revealed by reporting the normalized complex resistivity as a function of magnetic field, at fixed temperature and different frequencies. In Fig.(1.18) we report these data at $T = 15$ K, but similar results are obtained at all temperatures [134]. From this figure, it is immediately apparent that the straightforward application of a single-gap model, such as the CC model in its original formulation, leads to considerable contradictions. First of all, should one identify the initial, B-linear part of ρ_1 at the highest frequency with the flux flow resistivity ρ_{ff}, in analogy with the field-sweeps in YBCO, the resulting H_{c2} as obtained from the linear extrapolation depicted in Fig.(1.18) would be a factor 1.5-2 lower than H_{c2} independently measured on the same sample by dc resistivity [135]. Second, at low fields and high frequency there is a steep increase in $\rho_2(H)$, up to a smoothly temperature-dependent field H_1, as reported in Fig.1.20. Taking the vortex motion as the only source of response, this is possible only with the assumption that $\nu_0 \approx$ 15 GHz, and strongly field-dependent. However, if this were true, one should observe a large variation (as a function of frequency) of $\rho_1(H)$ in the same

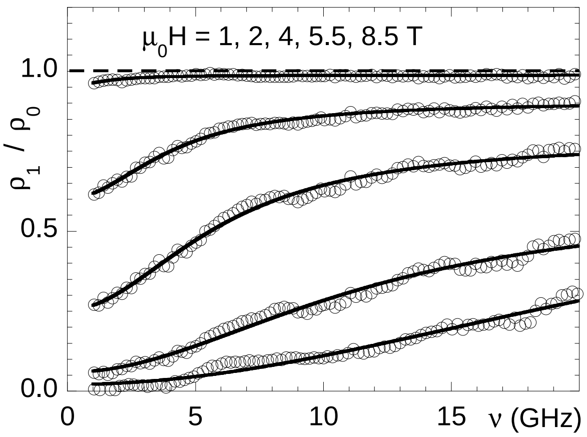

Figure 1.16: Frequency dependence of ρ_1 in MgB$_2$, at $T = 10$ K and different magnetic fields (analogous to Fig.1.9). Remarkably, a blind fit with Eq.(1.5) gives good agreement (thick continuous lines). However the resulting parameters exhibit very contradictory field and temperature dependences, see text and Fig.1.17.

field and frequency ranges. There is no indication of such a strong difference between the experimental curves $\rho_1(H)$ measured at different frequencies for $\nu > 10$ GHz, indicating that typical vortex frequencies are not placed in this range. The steep increase of the imaginary response, followed by the more gradual decrease, is then more likely ascribed to an unconventional increase of the screening length, as it could be given by the fast suppression of the superfluid fraction in the weak π band [136]. We finally note that, above a crossover field H_2, ρ_2 is nearly independent on frequency: there are at present no indications on the possible origins for this feature, so that in the following we confine the discussion to fields $H < H_2$.

We can thus conclude that swept-frequency measurements reveal a clearly richer physics of the vortex-state in MgB$_2$ than, e.g., in YBCO. Accordingly, the interpretation of the data must be based on more complex models.

In this perspective, it is interesting to compare the measured behaviors of $\rho_1(H)$ and $\rho_2(H)$ with the predictions of the model that takes into account both vortices and quasiparticles, Eqs.(1.6) and Fig.1.5, left panel (we assume that, according to literature, MgB$_2$ is an s-wave superconductor [137]). By comparing the measured data with the predicted curves, it is clear that the motion of vortices cannot take into account the whole observed high frequency behavior. Indeed, a rather large quasiparticle contribution (curves with small x_{s0}) is needed to obtain behaviors similar to those observed: it is seen from Fig.1.5, left panel, that (at high frequency: in Fig.1.5

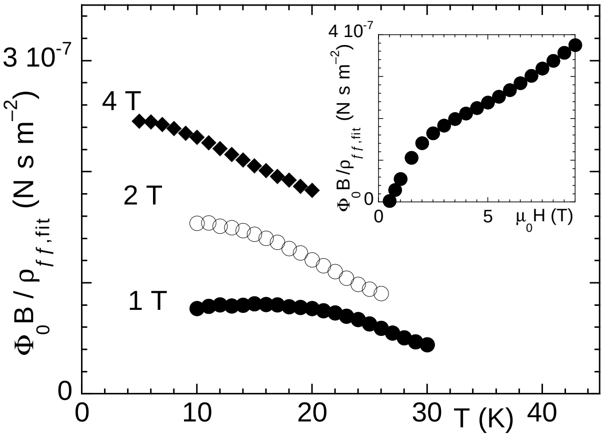

Figure 1.17: Field and temperature dependence of the ratio $\Phi_0 B/\rho_{ff,fit}$ as obtained from the MgB$_2$ data fitted through Eq.(1.5). This ratio should equals η. It is readily seen that both temperature and magnetic field dependences present very exotic behavior.

it is assumed $\nu \gg \nu_0$) $\rho_1(H)$ should increase approximately linearly with field while $\rho_2(H)$ should be more or less constant at low fields and then decrease approaching the upper critical field. Apart from the low field region ($H < H_1$), this behavior is rather similar to the measured one. We can then conclude that, provided a large quasiparticle contribution is taken into account, the behaviors observed could possibly be described in terms of rather simple one-band models for $H > H_1$. This result is fully consistent with spectroscopic measurements [81, 82] which show that the superfluid density of the π band decreases strongly with the magnetic field, nearly vanishing at a characteristic field H^*: the microwave response in the vortex state at low fields, where both gaps play a role, cannot be described by a singe gap model, while the higher field data can be nicely described by that model. This picture is reinforced by noting that both the temperature dependence and the numerical values of H_1 agree very well with those reported for H^* [81, 82, 83, 138].

We now show that the microwave resistivity above $H_1(T)$ quantitatively coincides with a model for a single-band superconductor, Eqs.(1.6), if the conductivity of the π band is taken as purely real.

We make some rather crude approximations in order to reduce the number of fitting parameters. First of all, we assume that above H_1 the residual $\pi-$band contribution to the superfluid can be neglected, so that the superfluid fraction $x_s(T,B)$ is related to the superfluid fraction of the σ band only, $x_{s,\sigma}(T,B) = N_{s,\sigma}/N_\sigma$ (that is, the superfluid volume density divided

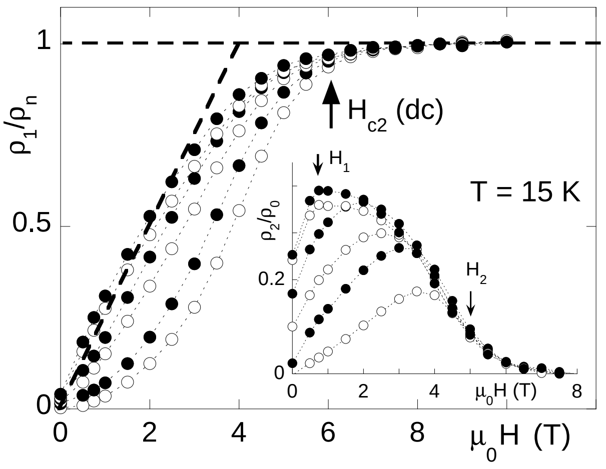

Figure 1.18: Field dependence of the complex resistivity at fixed frequencies ν =2, 5, 9, 12, 15, 18 GHz (frequency increases from the bottom curve to the top one) and $T = 15$ K in MgB$_2$. Main panel: ρ_1/ρ_0. The intersection of the dashed lines indicates the upper critical field as it would result from a naive application of a vortex motion model. Inset: ρ_2/ρ_0. Arrows indicate the field H_1 where the high-frequency imaginary resistivity reaches a maximum and the field H_2 where there is no more a clear frequency dependence in ρ_2.

by the total volume density of electrons in the σ band), through the relation $x_s(T,B) = Kx_{s,\sigma}(T,B)$, with $K = N_\sigma/(N_\sigma + N_\pi)$, being N_π the volume density of electrons in the π band. The penetration depth above H_1 becomes then $\lambda^2(T,B) = \lambda^2_{0,\sigma}/x_{s,\sigma}(T,B)$.

For what concerns the normal fluid resistivity $\rho_{nf} = 1/\sigma_{nf}$, we assume that, since the σ and π bands interact very weakly with each other [139], above H_1 one can write $\sigma_{nf} \simeq \sigma_{n,\pi} + [1 - x_{s,\sigma}(T,B)]\sigma_{n,\sigma}$. Using the independently measured [107, 140], temperature dependent H_{c2} anisotropy of our sample, the Gurevich model [141] yields $\sigma_{n,\sigma}/\sigma_{n,\pi} \simeq 0.25$. One then obtains, to a good approximation, $\rho_{nf}/\rho_n = 1$ in all the field and temperature region $H > H_1(T)$, and the T and B variations of $\nu_s(T,B)$ are then entirely determined by $x_s(T,B) = x_{s0}(T)(1-b)$, where the last equality comes from the single-gap-like behavior above H_1, $b = B/B_{c2}(T) \simeq H/H_{c2}(T)$ and $x_{s0}(T) = Kx_{s,\sigma}(B = 0,T)$ is the (extrapolated) zero field value[5] of x_s. Once this general frame has been established, it is possible to extract from the data, by means of a selfconsistent procedure reported in the Appendix, the temperature dependent σ-band superfluid fraction $x_{s0}(T)$, the temperature

---

[5] We remark that $x_{s0}(T)$ is different from the value that is obtained through experiments that measure the superfluid density at $B = 0$, being in that case $x_s^{meas}(B = 0,T) = x_{s,\sigma}(B = 0,T) + x_{s,\pi}(B = 0,T)$

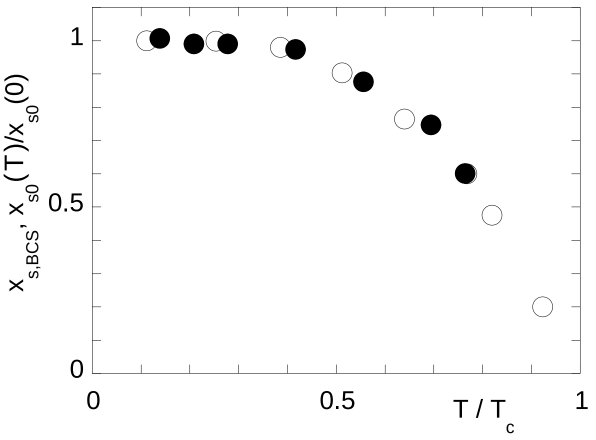

Figure 1.19: Full dots: temperature dependence of the zero-field $\sigma-$band superfluid fractional density obtained from the selfconsistent fitting procedure. Open symbols are calculations with the standard BCS relation [11] using gap values from [142].

dependent upper critical field $H_{c2}(T)$, the vortex motion resistivity $\rho_v(\nu)$ and, consequently, the characteristic frequency ν_0. We now discuss those quantities. In Fig.1.19 we report the behavior of $x_{s0}(T)$, normalized to the lowest temperature value $x_{s0}(T = 5\text{ K})$. We compare the T dependence of $x_{s0} = Kx_{s,\sigma}(B = 0, T)$, with $x_{s,\sigma}(B = 0, T)$ as obtained using the expressions of the BCS theory [11], and the values of the gap $\Delta_\sigma(T)$ measured by point contact spectroscopy [142]. The theoretical calculation and data points from our microwave measurements agree very well, giving a strong support to the consistency of the analysis here performed, and adding evidence that the temperature dependence of the zero-field superfluid fraction in the σ band follows a rather conventional behavior.

Similarly, we obtain values of the upper critical field H_{c2} (Fig. 1.20) in nearly perfect agreement with values obtained independently from the *dc* measurements [136], giving further confirmation on the reliability and consistency of the underlying model. We remark that this is a nontrivial result: previous analysis have never been able to describe the microwave data using the same parameters obtained from low frequency measurements. In particular, the upper critical field was found to be field dependent [143] or anomalous field dependencies for the vortex viscosity were invoked [76].

Finally we report in Fig.1.21 the vortex motion complex resistivity, isolated from the experimental data by means of the selfconsistent procedure. We remark that now those data are not flawed, as the raw data, by the presence of the strong contribution of the π band, or of the overall field depen-

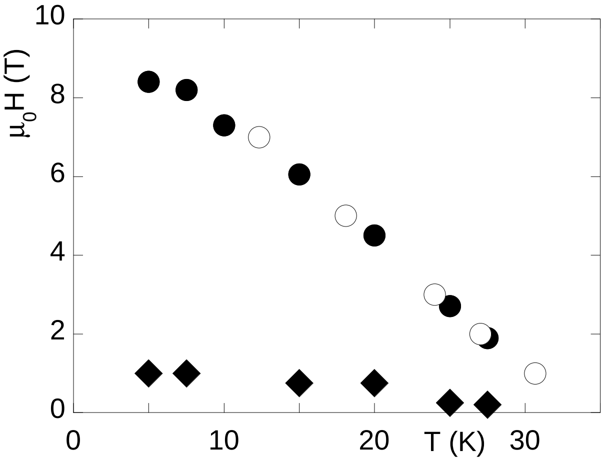

Figure 1.20: $H - T$ phase diagram in MgB_2. Open circles: H_{c2} from *dc* measurements. Full dots, H_{c2} from the selfconsistent fitting procedure. Diamonds, H_1.

dence of the superfluid concentration (see the Appendix). We then fitted all the pairs of curves $\mathrm{Re}[\tilde{\rho}_v]/\rho_n(\nu)$, $\mathrm{Im}[\tilde{\rho}_v]/\rho_n(\nu)$ to Eqs.(1.5) at all given temperatures and fields, using ϵ and ν_0 as fitting parameters ($\rho_{ff}/\rho_n = H/H_{c2}$ is determined by the value of H_{c2} obtained previously). A typical fit for $T = 15$ K and $\mu_0 H = 3$ T is reported in Fig.(1.21). We find, consistently with the indication given by the small frequency dependence of ρ_1, that ν_0 never exceeds 10 GHz, for any temperature and field. In addition, we find a rather strong field dependence of ν_0 at different temperatures, as reported in Fig.(1.22). This is an indication, in agreement with previous findings [143], of the collective nature of the pinning forces in this material. This conclusion is also supported by the low temperatures collapsing of all curves $\nu_0(b)$, with $b = B/B_{c2}(T)$.

Summarizing, we have shown that multifrequency measurements are a key factor to elucidate the role of quasiparticle, superfluid and vortex motion in the overall transport properties of MgB_2 in the vortex state. By suppressing the π band contribution with a sufficiently strong magnetic field it has been possible to evaluate the σ band superfluid density, the upper critical field and the characteristic vortex frequency.

1.4.3 $SmBa_2Cu_3O_{7-\delta}$

The case of $SmBa_2Cu_3O_{7-\delta}$ (SmBCO) is somehow similar to the case of MgB_2, in that an additional, strong contribution different from vortex motion affects the complex resistivity. In this Subsection we report measure-

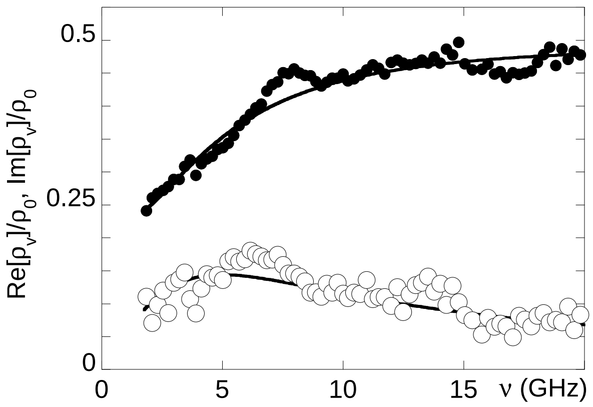

Figure 1.21: Contribution of the vortex motion to the overall field-dependent complex resistivity in MgB_2, isolated as described in the text. Full dots, $\mathrm{Re}[\rho_v]$; open circles, $\mathrm{Im}[\rho_v]$. Continuous lines are simultaneous fits by Eqs.(1.5).

ments of the complex resistivity for temperatures down to 65 K in moderate fields $\mu_0 H$ <0.8 T and at the high operating frequency $\omega/2\pi$ = 48 GHz. Most of the measurements are thus taken below the irreversibility line of SmBCO [144, 145]. Typical field sweeps for the variation of the complex resistivity at various sample temperatures are reported in Fig.(1.23). The data here reported are representative of the behavior observed in other SmBCO films measured under the same conditions and in similar temperature and field ranges. We list the most relevant experimental features that will determine the discussion of the data, and we specifically compare them to the behavior of the parent compound YBCO.

At all temperatures, $\Delta\rho_1/\rho_0$ exhibits a pronounced downward curvature at low fields, followed by an approximately linear increase at higher fields. By contrast, $\Delta\rho_2/\rho_0$ never shows a linear variation. Moreover, $\Delta\rho_2/\rho_0$ changes from positive to negative as the temperature increases, but without changing the curvature of the data. Those considerations can be put on more quantitative grounds by plotting the data as a function of $\sqrt{H}$, as reported in Fig.1.24. It is seen that $\Delta\rho_2/\rho_0$ is well approximated by a straight line, which corresponds to a $\sim \sqrt{H}$ dependence, while upward curvature in $\Delta\rho_1/\rho_n$ *vs.* $\sqrt{H}$ indicates the presence of both a square root and a linear term in the H dependence. Summarizing, to the best of our experimental accuracy, the complex resistivity in SmBCO can be described by $\Delta(\rho_1 + \mathrm{i}\rho_2)/\rho_0 \simeq [a_1(T) + \mathrm{i}a_2(T)]\sqrt{\mu_0 H} + b_1(T)\mu_0 H$.

With respect to YBCO we then encounter two main differences: the field dependence, which has a strong sublinear component in the entire temper-

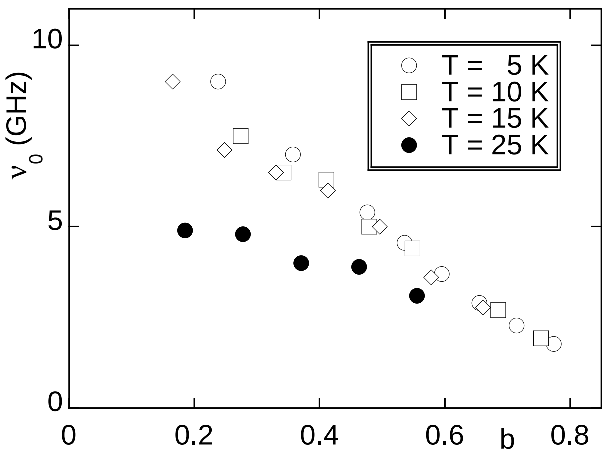

Figure 1.22: Reduced field dependence of the vortex characteristic frequency ν_0 in MgB$_2$ at various temperatures. The reduced field $b = B/B_{c2}$.

ature range explored, and the very relevant increase of the imaginary part in even moderate fields. In order to discuss the data, in analogy to the discussion on the other materials here investigated, we first tentatively ascribe the observed behavior to the vortex motion alone. For the purpose of the discussion, it is sufficient to focus on the data at low enough temperature, that is below the irreversibility line, where creep can be neglected. We then consider for the preliminary discussion Eqs.(1.7). In the conventional data analysis the superfluid density (or, which is the same, the London penetration depth) does not change appreciably with the field, and pinning affects mostly the imaginary part of the response. One might then be tempted to assign the difference between YBCO and SmBCO simply to a much stronger, or different, pinning in SmBCO. Making use of the vortex-motion-only expressions, Eqs.(1.7), one would directly calculate the pinning frequency from the data[6] as: $\nu_p^{calc} = \nu \frac{\Delta\rho_2}{\Delta\rho_1}$. Proceeding further within the same framework, once the tentative ν_p has been calculated the viscosity follows immediately by calculating $\frac{\Phi_0 B}{\Delta\rho_1}\frac{1}{1+(\nu_p/\nu)^2}$, see Eqs.(1.7). However, within this framework we would obtain a field-dependent vortex viscosity, in particular $\sim \sqrt{B}$, at odds with the measured vortex viscosity in YBCO. The procedure is illustrated in Fig.1.25, where the as-calculated vortex parameters are reported at one temperature.

Then, it would appear that both the pinning mechanism (implicit in ν_p^{calc}) and the electronic state (implicit in the calculated vortex viscosity

---

[6] This kind of analysis has been widely used in the past in various HTCS, as reviewed in [35].

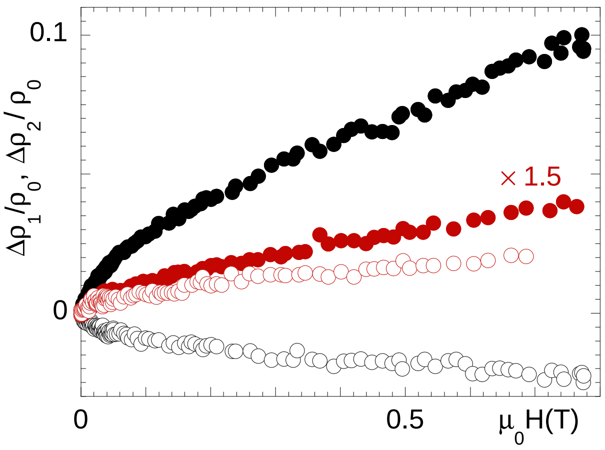

Figure 1.23: Field dependence of the complex resistivity changes in SmBCO (sample Sm2) at two temperatures. Black symbols, $T = 82$ K. Red symbols, $T = 71$ K. A sublinear component is evident both in $\Delta\rho_1/\rho_0$ (full dots) and in $\Delta\rho_2/\rho_0$ (open circles). Note the large values and the sign change of $\Delta\rho_2/\rho_0$ with increasing temperature. $\Delta\rho_1/\rho_0$ at 71 K has been scaled to avoid crowding.

η^{calc}) are very different in SmBCO and YBCO. This conclusion does not appear very reasonable, due to the structural, electrical and superconducting similarities between the two compounds. In particular, while pinning may well be sample-dependent, the much different field behavior of the vortex viscosity put doubts on the correctness of the simple model used.

We now propose a possible alternative explanation for our data. Since, as a first approximation, the vortex motion resistivity at low fields should be proportional to the number of flux lines, that is to the induction $B \simeq \mu_0 H$, we tentatively assume that only the linear part of our data is due to the vortex motion. In this case, we deduce from the data that there is almost no vortex motion contribution to the imaginary resistivity. This is exactly the behavior as exhibited by YBCO at the same frequency, that shows free flux flow at 48 GHz.

We have now to identify the physical mechanism responsible for the $\sim \sqrt{H}$ part of the real and imaginary resistivity and its peculiar features (in particular, the change of sign of $\Delta\rho_2(H)$ with increasing temperature). As shown in Fig. 1.5, right panel, the change of sign of $\Delta\rho_2(H)$ with increasing temperature is a signature of the field-dependent superfluid depletion, while the $\sim \sqrt{H}$ dependence points to a specific electronic state, namely a superconducting gap with lines of nodes. Thus, it is possible to compare theory and experiment. Making use of Eq.(1.6), we can expand for low fields (small

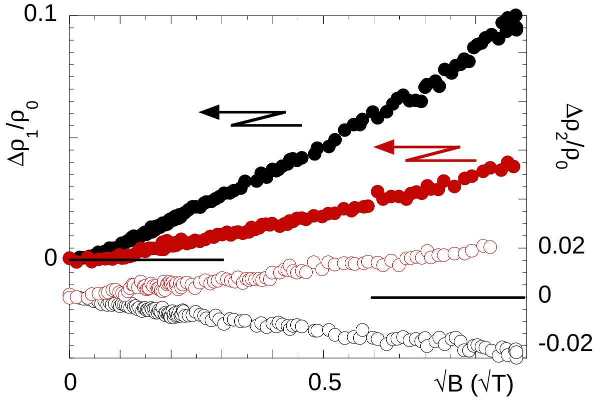

Figure 1.24: Same data of Fig.(1.23), replotted *vs.* $\sqrt{H}$. Left scale, $\Delta\rho_1/\rho_0$. Right scale, $\Delta\rho_2/\rho_0$. Symbols as in Fig.(1.23). It clearly appears that $\Delta\rho_2/\rho_0 \propto \sqrt{H}$.

$H/H_{c2} \simeq B/B_{c2}$) and we obtain explicit expressions for the coefficients $a_1(T)$ and $a_2(T)$. Those expressions contain several temperature-dependent quantities, for which we believe it is appropriate to use the simplest possible model: we take the superfluid fraction $x_{s0}(T) = \left(1 - t^2\right)$, which is a recognized approximation in a very wide temperature range for HTCS [64], and the pair breaking field $B_{pb} \propto B_{c2}(T)$, as theoretically suggested [95, 96], so that $B_{pb} = B_{pb0}\left(1 - t^2\right)$, with $t = T/T_c$. In order to gain qualitative information, we do not attempt to insert some temperature dependence in the quasiparticle scattering time τ_{qp}, that we use as a free parameter. As can be seen in Fig.1.26, the fits reproduce the shape, height, width of the curve given by the experimental data, including the temperature of change of sign for a_2. The resulting $\tau_{qp} \simeq 0.7$ ps compares well to the highest values reported in YBCO, e.g., 0.2 ps at ≈ 80 K as obtained from microwave measurements crystals [64] and to 0.5 ps at ≈ 80 K as obtained from millimeter-wave interferometry in YBCO film [65]. Even if the model can certainly be improved (e.g., by considering a temperature-dependent τ_{qp}), the substantial agreement with the data led us to conclude that the microwave resistivity in the vortex state observed in our SmBCO samples is strongly affected by the field-induced superfluid depletion, and that the differences between different samples of YBCO and SmBCO are determined by mere quantitative differences in τ_{qp}.

Coming back to the fluxon dynamics, once the temperature dependence of the carrier conductivity has been assessed from the above described fit, one can extract the vortex viscosity in a wide temperature range[7]. The

---

[7] At low temperature the slope b_1 directly yields η, but approaching T_c the quasiparticle

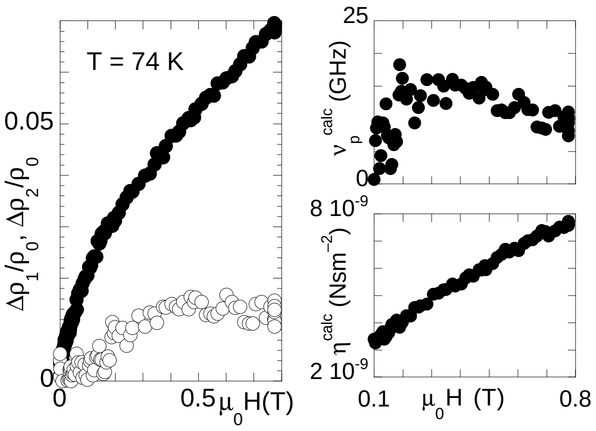

Figure 1.25: Left panel: complex resistivity changes at 74 K in sample Sm1. Right panels: field dependence of the calculated vortex parameters ν_p^{calc} and η^{calc}, as they would result from the conventional framework for vortex-state complex resistivity. The calculated viscosity η^{calc} presents a strong field dependence, at odds with models and with experimental data in YBCO.

so-obtained data points for the vortex viscosity are reported in Fig.1.27. Both numerical values and temperature dependences compare favorably to similar data in YBCO (Fig. 1.13), adding evidence that the vortex motion contribution has been correctly identified.

1.4.4 General remarks

As we have shown in this study, the physics of superconductors in the vortex state can take advantage from investigations at microwave frequencies. However, in order to assess with some confidence the various mechanisms responsible for the microwave response, it is necessary to combine temperature, field and frequency dependent measurements. This is especially needed in the two-gap superconductor MgB$_2$, where single frequency measurements are not able to assess the nature of the strong anomaly in the low-field response.

By the combined measurements here reported, it has been shown that, in all cases here investigated, the correctly identified vortex motion contribution follows to a great accuracy the conventional models. In particular, the high frequency regime always coincides with conventional flux flow (above H^* in MgB$_2$): this is a remarkably noticeable point, since it implies that, in the field and temperature ranges studied, the dominant excitations inside the

---

screening length comes into play and a correction is needed, see Eq.(1.4).

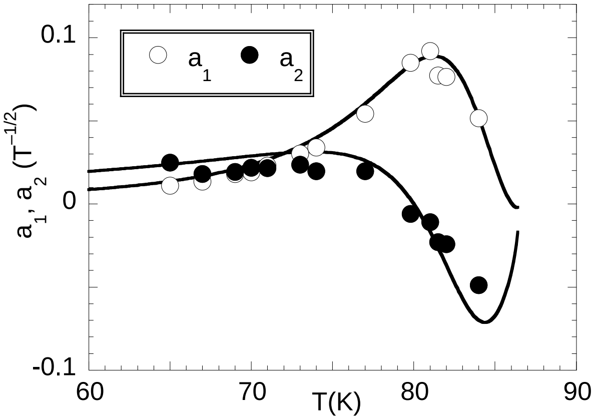

Figure 1.26: Plot of the coefficients $a_1(T)$ and $a_1(T)$. Continuous lines are simultaneous fits with the pair breaking expression described in the text. Details are reported in [146].

vortex cores in the materials examined are conventional quasiparticle excitations, as indicated by the temperature dependence and field independence of the vortex viscosity. In order to emphasize this point, we plot in Fig. 1.27 the vortex viscosity as measured by us in YBCO and SmBCO thin films and the depinning frequency obtained by us in YBCO films, together with data obtained in YBCO crystals by multifrequency cavity measurements [43]. It is immediately seen that the vortex viscosity has the same behavior in YBCO and SmBCO, films and crystals. Moreover, the data for different materials scale one onto the other with mere numerical factors of order unity, consistently with the viscosity given by the standard expression $\eta = \Phi_0 B_{c2}/\rho_n$. Correctly, the depinning frequency in YBCO appears to be different in films and in crystals, indicating that defects in samples (or size effects) play a role. We especially emphasize this point, in comparison to earlier studies (see the early review in [35]) that reported the very anomalous sample independent depinning frequency and sample dependent vortex viscosity, quite the opposite of the expected behavior.

In fact, a second important indication that emerges from our measurements is that it is in general not appropriate to neglect the field dependence of the superfluid density and quasiparticle density of states in the materials under study: albeit coming from different physical origins, the superfluid density results to be much weaker than in conventional superconductors upon the application of an external magnetic field. This latter feature seems to be governed by the (sample-dependent) quasiparticle scattering time in RE-BCO. In MgB_2 the low fields behavior is only qualitatively understood, so that this material appears to be most interesting for future studies. In

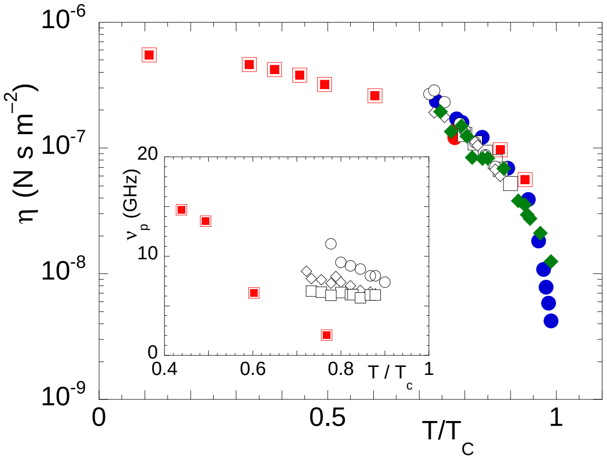

Figure 1.27: Temperature dependence of the vortex viscosity η obtained in this study in YBCO (data and symbols as in Fig.1.13) and SmBCO films (green filled diamonds), compared to data obtained in crystals at 19.1 GHz (red squares, from [43]). The data in SmBCO have been multiplied by 2. All the data collapse on the same curve, indicating that the same electronic mechanisms take place in the vortex core. Inset: depinning frequency in YBCO films (sample Y3, same data and symbols as in Fig.1.12) compared to measurements at 19.1 GHz in single crystals (red squares, from [43]).

particular, there is at present no consensus on a representation of the vortex dynamics when both gaps are effective, which is then a promising field for investigation.

1.5 CONCLUSION

We have extensively investigated the experimental microwave response of innovative superconductors (cuprates and MgB_2) combining resonant and swept-frequency techniques. We have shown that this combination allows for the identification of the major differences between those superconductors and the conventional, metallic superconductors. The main difference resides in the weakness of the superfluid density with respect to an applied magnetic field both in cuprates and MgB_2, coming however from different physics. By contrast, the vortex motion contribution appears to be well described by conventional models (above H^* in MgB_2).

Appendix A: Selfconsistent fitting procedure in MgB_2

Here we describe the selfconsistent fitting procedure for the swept-frequency data in MgB_2. We refer to the general expressions, Eqs.(1.4).
The values of x_{s0} and H_{c2} for each temperature can be obtained as follows. As a first step, we notice that, if $\frac{\nu}{\nu_s(B,T)} = 2\left(\frac{\lambda(B,T)}{\delta_{nf}(B,T)}\right)^2$ is known at any fixed temperature and field, $r_1(\nu, B, T)$ and $r_2(\nu, B, T)$ can be obtained from the measured ρ_1/ρ_n and ρ_2/ρ_n by inverting Eqs.(1.4). Although the frequency, temperature and field dependence of r_1 and r_2 are not known *a priori*, the high frequency limit of r_1 is known: at high enough frequency Eq.(1.5) gives $\mathrm{Re}[\rho_v]/\rho_n \to \rho_{ff}/\rho_n = b$, with $b = B/B_{c2}(T) \simeq H/H_{c2}(T)$, having assumed the validity of the Bardeen Stephen expression [13] for the flux flow resistivity. We then choose a given temperature T_0 and calculate, for any value of H, a value of $\nu_s(B,T)$ using tentative values of $x_{s0}(T_0)$ and $H_{c2}(T_0)$ and $x_s(H,T_0) = x_{s0}(T_0)(1-b)$. We then obtain for all fields $r_1(\nu, B, T_0)$ inverting Eqs.(1.4) and we check that they approach a constant value at high frequency. The values of $x_{s0}(T_0)$ and $H_{c2}(T_0)$ are then changed until, for all fields, the high frequency value for r_1 is equal to $b = H/H_{c2}(T_0)$. Thus, *having assumed only the high frequency limit of* r_1, $r_1(\nu)$ and $r_2(\nu)$ at various fields and temperatures are obtained. Since $\frac{\lambda(B,T_0)}{\delta_{nf}(B,T_0)}$ has already been selfconsistently determined at each temperature T_0, we can isolate the *pure vortex motion complex resistivity* $\mathrm{Re}[\rho_v(\nu)]$ and $\mathrm{Im}[\rho_v(\nu)]$ at various fields and temperatures. Those curves can then be fitted to Eq.(1.5) to get the vortex parameters.

Acknowledgments

This work has been partially supported by INFM under the national projects PRA-H.O.P and PRA-U.M.B.R.A., and by MIUR under a FIRB project “Strutture Semiconduttore/Superconduttore per l’elettronica integrata”. We thank V. Ferrando and C. Ferdeghini for supplying the MgB_2 sample, C. Camerlingo for YBCO sample Y4 and M. Boffa and A.M. Cucolo for the remaining YBCO and SmBCO samples. We acknowledge useful discussions with S. Anlage, M. Ausloos, M.W. Coffey, R. Fastampa, M. Giura, J. Halbritter, A. Maeda, R. Marcon, D. Neri, D. Oates, R. Wördenweber.

Bibliography

[1] Biondi, M. A.; Forrester, A. T.; Garfunkel, M. P.; Satterthwaite, C. B. *Rev. Mod. Phys.* 1958, **30** 1109.

[2] Biondi, M. A.; Garfunkel, M. P. *Phys. Rev.* 1959, **116** 853.

[3] D'Aiello, R.V.; Freedman, S.J. *Phys. Rev. Lett.* 1969, **22**, 515.

[4] Lehoczky, S.L.; Briscoe, C.V. *Phys. Rev. Lett.* 1969, **23**, 695.

[5] Lehoczky, S.L.; Briscoe, C.V. *Phys. Rev. B* 1971, **4**, 3938.

[6] Pippard, A. B. *Proc. R. Soc.* 1947, **A191**, 399.

[7] Pippard, A. B. *Proc. R. Soc.* 1950, **203**, 98.

[8] Waldram, J. R. *Adv. Phys.* 1964 **49**, 1

[9] Rosenblum, B.; Cardona, M. *Phys. Lett.* 1964, **9**, 220.

[10] Rosenblum, B.; Cardona, M. *Phys. Rev. Lett.* 1964, **12**, 657.

[11] Tinkham, M. *Introduction to Superconductivity 2nd edition*; McGraw-Hill: New York, US, 1996.

[12] see, e.g., Abrikosov, A. A. *Fundamentals of the Theory of Metals*; North-Holland, 1988.

[13] Bardeen, J.; Stephen, M. J. *Phys. Rev.* 1965 **140**, A1197.

[14] de Gennes, P. G. *Superconductivity of Metals and Alloys*; Addison-Wesley.

[15] Kim, Y. B. ; Stephen, M. J. In *Superconductivity*; Parks, R. D., Ed., Marcel Dekker, Inc. : New York, US, 1969; pp 1107.

[16] Campbell, A. M.; Evetts, J. E. *Adv. Phys.* 1972 **21**, 199

[17] Suhl, H. *Phys. Rev. Lett.* 1965, **14**, 226.

[18] Matsuda, Y.; Ong, N. P.; Yang, Y. F.; Harris, J. M.; Peterson, J. B. *Phys. Rev. B* 1994, **49**, 4380.

[19] Kopnin, N. B. ; Vinokur, V. M. ; *Phys. Rev. Lett.* 1998, **81**, 3952.

[20] Sonin, E. B. *Phys. Rev. B* 2001, **63**, 054527.

[21] Han, J. H. ; Kim, J. S. ; Kim, M. J.; Ping Ao *Phys. Rev. B* 2005, **71**, 125108.

[22] Gittleman, J. I.; Rosenblum, B. *Phys. Rev. Lett.* 1966, **16**, 734.

[23] Wu, D. H.; Shridar, S. *Phys. Rev. Lett.* 1990, **65**, 2074.

[24] Yeh, N.-C. *Phys. Rev. B* 1991, **43**, 523.

[25] Golosovsky, M.; Naveh, Y.; Davidov, D. *Phys. Rev. B* 1992, **45**, 7495.

[26] Huang, M. X.; Bhagat, S. M.; Findicoglu, A. T.; Venkatesan, T.; Manheimer, M. A.; Tyagi, S. *Physica C* 1992, **193**, 421.

[27] Owliaei, J. ; Sridhar, S. ; Talvacchio, J. *Phys. Rev. Lett.* 1992, **69**, 3366.

[28] Pambianchi, M. S. ; Wu, D. H. ; Ganapathi, L. ; Anlage, S. M. *IEEE Trans. Appl. Supercond.* 1993, **3**, 2774.

[29] Silva, E.; Marcon, R.; Matacotta, F. C. *Physica C* 1993, **218**, 109.

[30] Golosovsky, M.; Tsindlekht, M.; Chayet, H.; Davidov, D. *Phys. Rev. B* 1994, **50**, 470; *ibidem* 1995, **51**, 12062.

[31] Revenaz, S.; Oates, D. E.; Labbé-Lavigne, D.; Dresselhaus, G.; Dresselhaus, M. S. *Phys. Rev. B* 1994, **50**, 1178.

[32] Morgan, D. C. ; Zhang Kuan ; Bonn D. A. , Liang Ruixing ; Hardy, W. N. ; Kallin, C. ; Berlinsky, A. J. *Physica C* 1994, **235-240**, 2015.

[33] Parks, B.; Spielman, S.; Orenstein, J.; Nemeth, D. T.; Ludwig, F.; Clarke, J.; Marchant, P.; Lew, D. J. *Phys. Rev. Lett.* 1995, **74**, 3265.

[34] Wu, D. H.; Booth, J. C.; Anlage, S. M. *Phys. Rev. Lett.* 1995, **75**, 525.

[35] Golosovsky, M.; Tsindlekht, M.; Davidov, D. *Supercond. Sci. Technol.* 1996, **9**, 1 and references therein.

[36] Belk, N.; Oates, D. E.; Feld, D. A.; Dresselhaus, G.; Dresselhaus, M. S. *Phys. Rev. B* 1996, **53**, 3459.

[37] Belk, N.; Oates, D. E.; Feld, D. A.; Dresselhaus, G.; Dresselhaus, M. G. *Phys. Rev. B* 1997, **56**, 11966.

[38] Lütke-Entrup, N.; Plaçais, B.; Mathieu P.; Simon, Y. *Phys. Rev. Lett.* 1997, **79**, 2538.

[39] Ong, N. P.; Wu, H. *Phys. Rev. B* 1997, **56**, 458.

[40] Hanaguri, T.; Tsuboi, T.; Tsuchiya, Y.; Sasaki, K.; Maeda, A. *Phys. Rev. Lett.* 1999, **82**, 1273.

[41] Rogai, R.; Marcon, R.; Silva, E.; Fastampa, R.; Giura, M.; Sarti, S.; Boffa, M.; Cucolo, A. M. *Int. J. Mod. Phys. B* 2000, **14**, 2828.

[42] Silva, E.; Fastampa, R.; Giura, M.; Marcon, R.; Neri, D.; Sarti, S. *Supercond. Sci. Technol.* 2000, **13**, 1186.

[43] Tsuchiya, Y.; Iwaya, K.; Kinoshita, K.; Hanaguri, T.; Kitano, H.; Maeda, A.; Shibata, K.; Nishizaki, T.; Kobayashi, N. *Phys. Rev. B* 2001, **63**, 184517.

[44] Silva, E.; Marcon, R.; Muzzi, L.; Pompeo, N. ; Fastampa, R.; Giura, M.; Sarti, S.; Boffa, M.; Cucolo, A. M.; Cucolo, M. C. *Physica C* 2004, **404**, 350.

[45] Parks, B.; Orenstein, J.; Mallozzi, R.; Nemeth, D. T.; Ludwig, F.; Clarke, J.; Merchant, P.; Lew, D. J.; Bozovic, I.; Eckstein, J. N. *J. Phys. Chem. Solids* 1995, **56**, 1815.

[46] Mallozzi, R.; Orenstein, J.; Eckstein, J. N.; Bozovic, I. *Phys. Rev. Lett.* 1998, **81**, 1485.

[47] Blatter G.; Feigel'man M. V.; Geshkenbein V. B.; Larkin A. I.; Vinokur V. M. *Rev. Mod. Phys.* 1994, **66**, 1125.

[48] Brandt, E. H. *Rep. Prog. Phys.* 1995, **58**, 1465.

[49] Pakulis, E. J.; Osada, T. *Phys. Rev. B* 1988, **37**, 5940.

[50] Marcon, R.; Fastampa, R.; Giura, M.; Matacotta, C. *Phys. Rev. B* 1989, **39**, 2796.

[51] Giura, M.; Marcon, R.; Fastampa, R. *Phys. Rev. B* 1989, **40**, 4437.

[52] Giura, M.; Fastampa, R.; Marcon, R.; Silva, E. *Phys. Rev. B* 1990, **42**, 6228.

[53] Wosik, J.; Kranenburg, R. A.; Wolfe, J. C.; Selvamanickam, V.; Salama, K. *J. Appl. Phys.* 1991, **69**, 874.

[54] Wosik, J.; Xie, L. M.; Chau, R.; Samaan, A.; Wolfe, J. C. *Phys. Rev. B* 1993, **47**, 8968.

[55] Fastampa, R.; Giura, M.; Marcon, R.; Silva, E. In *Studies of High Temperature Superconductors*; Narlikar, A. V.; Ed., Nova Science: New York, US, 1996; Vol. 17, pp 115-145.

[56] Halbritter, J. *J. Supercond.* 1995, **8**, 691.

[57] Gurevich, A. *Phys. Rev. B* 1992, **46**, 3187.

[58] Gurevich, A. *Phys. Rev. B* 2002, **65**, 214531.

[59] Xin, H.; Oates, D. E.; Dresselhaus, G.; Dresselhaus, M. S. *Phys. Rev. B* 1990, **65**, 214533.

[60] Lee, Sheng-Chiang ; Lee, Su-Young ; Anlage, Steven M. *Phys. Rev. B* 2005, **72**, 024527.

[61] Gaganidze, E.; Heidinger, R.; Halbritter, J.; Shevchun, A.; Trunin, M.; Schneidewind, H. *J. Appl. Phys.* 2003, **93**, 4049.

[62] Hardy, W. N.; Bonn, D. A.; Morgan, D. C.; Liang, Ruixing; Zhang, Kuan *Phys. Rev. Lett.* 1993, **70**, 3999.

[63] Mao, Jian ; Wu, D. H.; Peng, J. L.; Greene, R. L.; Anlage, S. M. *Phys. Rev. B* 1995, **51**, 3316.

[64] Bonn, D. A.; Liang, R.; Riseman, T. M.; Baar, D. J.; Morgan, D. C.; Zhang, K.; Dosanjh, P.; Duty, T. L.; MacFarlane, A.; Morris, G. D.; Brewer, J. H.; Hardy, W. N.; Kallin, C.; Berlinsky, A. J. *Phys. Rev. B* 1993, **47**, 11314.

[65] Nagashima, T.; Hangyo, M.; Nakashima, S.; Murakami, Y. In *Adv. in Superconductivity VI*; Fujita, T.; Shiohara, Y.; Eds.; Springer-Verlag: Tokyo, JP, 1994; pp 209-212.

[66] Jakobs, T.; Sridhar, S.; Rieck, C. T.; Scharnberg, K.; Wolf, T.; Halbritter, J. *J. Phys. Chem. Solids* 1995, **56**, 1945.

[67] Gao, F. ; Carr, G. L. ; Porter, C. D. ; Tanner, B. D. ; Williams, G. P. ; Hirschmugl, C. J. ; Dutta, B. ; Wu, X. D. ; Etemad, S. *Phys. Rev. B* 1996, **54**, 700.

[68] Nagamatsu, J.; Nakagawa, N.; Muranaka, T.; Zenitani, Y.; Akimitsu, J. *Nature* (London) 2001, **410**, 63.

[69] Bouquet, F.; Fisher, R. A.; Phillips, N. E. ; Hinks, D. G.; Jorgensen, J. D. *Phys. Rev. Lett.* 2001, **87**, 047001.

[70] Iavarone, M.; Karapetrov, G.; Koshelev, A. E.; Kwok, W. K.; Crabtree, G. W.; Hinks, D. G.; Kang, W. N.; Choi, Eun-Mi; Hyun Jung Kim; Kim, Hyeong-Jin ; Lee, S. I. *Phys. Rev. Lett.* 2002, **89**, 187002.

[71] Gonnelli, R. S.; Daghero, D.; Ummarino, G. A.; Stepanov, V. A.; Jun, J.; Kazakov, S. M.; Karpinski, J. *Phys. Rev. Lett.* 2002, **89**, 247004.

[72] Kim, Mun-Seong ; Skinta, John A.; Lemberger, Thomas R.; Kang, W. N.; Kim, Hyeong-Jin ; Choi, Eun-Mi ; Lee, Sung-Ik *Phys. Rev. B* 2002, **66**, 064511.

[73] Jin, B. B.; Klein, N.; Kang, W. N.; Kim, Hyeong-Jin; Choi, Eun-Mi; Lee, Sung-Ik; Dahm, T.; Maki, K. *Phys. Rev. B* 2002, **66**, 104521.

[74] Ghigo, G.; Botta, D.; Chiodoni, A.; Gozzelino, L.; Gerbaldo, R.; Laviano, F.; Mezzetti, E.; Monticone, E.; Portesi, C. *Phys. Rev. B* 2005, **71**, 214522.

[75] Dulčić, A.; Požek, M.; Paar, D.; Choi, Eun-Mi ; Kim, Hyun-Jung; Kang, W. N.; Lee, Sung-Ik *Phys. Rev. B* 2003, **67**, 020507(R).

[76] Shibata, A.; Matsumoto, M.; Izawa, K.; Matsuda, Y.; Lee, S.; Tajima, S. *Phys. Rev. B* 2003, **68**, 060501(R).

[77] Golubov, A. A.; Brinkman, A.; Dolgov, O. V. ; Kortus, J.; Jepsen, O. *Phys. Rev. B* 2002, **66**, 054524.

[78] Ohishi, K.; Muranaka, T.; Akimitsu, J.; Koda, A.; Higemoto, W.; Kadono, R. *J. Phys. Soc. Japan* 2003, **72**, 29

[79] Serventi, S.; Allodi, G.; De Renzi, R.; Guidi, G.; Romanò L.; Manfrinetti, P.; Palenzona, A.; Niedermayer, Ch.; Amato, A.; Baines, Ch. *Phys. Rev. Lett.* 2004, **93**, 217003.

[80] Babaev, E. *Phys. Rev. Lett.* 2002, **89**, 067001.

[81] Eskildsen, M. R.; Kugler, M.; Tanaka, S.; Jun, J.; Kazakov, S. M.; Karpinski, J.; Fischer, Ø. *Phys. Rev. Lett.* 2002, **89**, 187003.

[82] Gonnelli, R. S.; Daghero, D.; Calzolari, A. ; Ummarino, G. A.; Dellarocca, V.; Stepanov, V. A.; Jun, J.; Kazakov, S. M.; Karpinski, J. *Phys. Rev. B* 2004, **69**, 100504(R).

[83] Cubitt, R.; Eskildsen, M. R.; Dewhurst, C. D. ; Jun, J.; Kazakov, S. M.; Karpinski, J. *Phys. Rev. Lett.* 2003, **91**, 047002.

[84] Jackson, J. D. *Classical Electrodynamics*; Wiley: New York, US, 1962.

[85] Portis, A. M.; WBlazey, K.; Muller, K. A.; Bednorz, J. G. *Europhys. Lett.* 1988, **5**, 467.

[86] Sonin, E. B.; Tagantsev, A. K. *Zh. Eksp. Teor. Fiz.* 1989, **95**, 994 [*Sov. Phys.-JETP* 1989, **68**, 572].

[87] Marcon, R.; Fastampa, R.; Giura, M.; Silva, E. *Phys. Rev. B* 1991, **43**, 2940.

[88] Coffey, M. W.; Clem, J. R. *Phys. Rev. Lett.* 1991, **67**, 386.

[89] Brandt, E. H. *Phys. Rev. Lett.* 1991, **67**, 2219.

[90] Sonin, E. B.; Tagantsev, A. K.; Traito, K. B. *Phys. Rev. B* 1992, **46**, R5830.

[91] Plaçais, B.; Mathieu, P.; Simon, Y.; Sonin, E. B.; Traito, K. B. *Phys. Rev. B* 1996, **54**, 13083.

[92] Coffey, M. W.; Clem, J. R. *Phys. Rev. B* 1992, **45**, 10527.

[93] Coffey, M. W.; Clem, J. R. *Phys. Rev. B* 1992, **46**, 11757.

[94] Coffey, M. W.; Clem, J. R. *Phys. Rev. B* 1993, **48**, 342.

[95] Volovik, G. E. *JETP Lett.* 1993, **58**, 469.

[96] Won, H.; Maki, K. *Phys. Rev. B* 1996, **53**, 5927.

[97] Yip, S. K.; Sauls, J. A. *Phys. Rev. Lett.* 1992, **69**, 2264.

[98] Nakai, N ; Miranoviç, P.; Ichioka, M.; Machida, K. *Phys. Rev. B* 2004, **70**, 100503(R).

[99] Dahm, T.; Graser, S.; Iniotakis, C.; Schopohl, N. *Phys. Rev. B* 2002, **66**, 144515.

[100] Laiho, R.; Lähderanta, E.; Safonchik, M.; Traito, K. B. *Phys. Rev. B* 2004, **69**, 094508.

[101] Silva, E.; Marcon, R.; Sarti, S.; Fastampa, R.; Giura, M.; Boffa, M.; Cucolo A. M. *Eur. Phys. J. B* 2004, **37**, 277.

[102] Beneduce, C.; Bobba F.; Boffa M.; Cucolo A. M.; Cucolo M. C.; Andreone A.; Aruta C.; Iavarone M.; Palomba F.; Pica G.; Salluzzo M.; Vaglio R. *Int. J. Mod. Phys. B* 1999, **13**, 1333.

[103] Neri, D.; Marcon, R.; Rogai, R.; Silva, E.; Fastampa, R.; Giura, M.; Sarti, S.; Cucolo, A. M.; Beneduce, C.; Bobba, F.; Boffa, M ; Cucolo, M.C. *Physica C* 2000, **341-348** 2679.

[104] Camerlingo, C.; Lissitski, M. P.; Russo, M.; Salvato, M.; presented at *INFMeeting, June 2002, Bari, Italy* (unpublished)

[105] Boffa, M. A.; Bobba, F.; Cucolo, A. M.; Monaco, R. *Int. J. Mod. Phys. B* 2003, **17**, 768.

[106] Boffa, M.; Cucolo, M. C.; Monaco, R.; Cucolo, A. M. *Physica C* 2003 **384**, 419.

[107] Ferrando, V.; Amoruso, S.; Bellingeri, E. ; Bruzzese, R.; Manfrinetti, P.; Marré, D.; Velotta, R.; Wang, X.; Ferdeghini, C. *Supercond. Sci. Technol.* 2003, **16**, 241.

[108] Collin, R. E. *Foundation for microwave engineering 2nd edition*; Electrical Engineering Series; McGraw-Hill International Series: Singapore, 1992.

[109] Sridhar, S. *J. Appl. Phys.* 1988, **63**, 159.

[110] Silva, E.; Lanucara, M.; Marcon, R. *Supercond. Sci. Technol.* 1996, **9**, 934.

[111] Beeli, P. *Physica C* 2000, **333**, 65 and references therein.

[112] Pompeo, N.; Marcon, R.; Silva, E. In *Applied Superconductivity 2003 - Proc. of VI European Conference on Applied Superconductivity, Sorrento, Italy, 14-18/9/2003*; Andreone, A.; Pepe, G. P.; Cristiano, R.; Masullo, G.; Eds.; Institute of Physics, Conference Series **181**; 2004; pp 2629-2634.

[113] Pompeo, N.; Marcon, R.; Méchin, L.; Silva, E. *Supercond. Sci. Technol.* 2005, **18**, 531.

[114] Klein. M ; Chaloupka, H.; Müller, G.; Orbach, S.; Piel, H.; Roas, B.; Schultz, L.; Klein, U.; Peiniger, M. *J. Appl. Phys.* 1990, **67**, 6940.

[115] Hartemann, P. *IEEE Trans. Appl. Supercond* 1992, **2**, 228.

[116] Hein, A. M.; Strupp, M.; Piel, H.; Portis, A. M.; Gross, R. *J. Appl. Phys.* 1994, **75**, 4581.

[117] Silva, E.; Lanucara, M.; Marcon, R. *Physica C* 1997, **276**, 84.

[118] Poole, C. P. *Electron Spin Resonance. A Comprehensive Treatise on Experimental Techniques*; Interscience: New York, US, 1967.

[119] Clem, J. R. ; Sanchez, A. *Phys. Rev. B* 1994, **50**, 9355.

[120] Xing, X. ; Heinrich, B. ; Zhou, Hu ; Fife, A. A. ; Cragg, A. R. *J. Appl. Phys.* 1994, **76**, 4244.

[121] Silva, E.; Lezzerini, A.; Lanucara, M.; Sarti, S.; Marcon, R. *Meas. Sci. Technol.* 1998, **9**, 275.

[122] Ceremuga, J.; Krupka, J.; Kosciuk, T. *J. Supercond.* 1995, **8**, 681.

[123] Mazierska, J. *J. Supercond.* 1997, **10**, 73.

[124] Silva, E.; in *Superconducting Materials: Advances in Technology and Applications*, ed by A. Tampieri and G. Celotti, World Scientific, pp. 279-306 (2000)

[125] Sarti, S.; Amabile, C.; Silva, E. (2004) COND-MAT/0406313

[126] Amabile, C.; Fastampa, R.; Giura, M.; Sarti, S.; Silva, E.; Ferrando, V.; Tarantini, C.; Ferdeghini, C. In *Applied Superconductivity 2003 - Proc. of VI European Conference on Applied Superconductivity, Sorrento, Italy, 14-18/9/2003*; Andreone, A.; Pepe, G. P.; Cristiano, R.; Masullo, G.; Eds.; Institute of Physics, Conference Series **181**; 2004; pp 1281-1288.

[127] Ikeda, R.; Ohmi, T.; Tsuneto, T. *J. Phys. Soc. Jpn.* 1991, **60**, 1051.

[128] Mikeska, H.-J.; Schmidt, H. *Z. Physik* 1970 **230**, 239.

[129] Schmidt, H. *Z. Phys* 1968, **216**, 336. Ibidem 1970, **232**, 443.

[130] Skocpol, W. J.; Tinkham, M. *Rep. Prog. Phys.* 1975, **38**, 1049.

[131] Klemm, R. A. *J. Low Temp. Phys.* 1974, **16**, 381.

[132] Dorsey, A. T. *Phys. Rev. B* 1991 **43**, 7575.

[133] Silva, E. *Eur. Phys. J. B* 2002, **27**, 497.

[134] Sarti, S.; Silva, E.; Amabile, C.; Fastampa, R.; Giura, M. *Physica C* 2004, **404**, 330.

[135] Ferrando, V.; Manfrinetti, P.; Marré, D.; Putti, M.; Sheikin, I.; Tarantini, C.; Ferdeghini, C. *Phys. Rev. B* 2003, **68**, 94517.

[136] Sarti, S.; Amabile, C.; Silva, E.; Giura, M.; Fastampa, R.; Ferdeghini, C.; Ferrando, V.; Tarantini, C. *Phys. Rev. B* 2005, **72**, 024542.

[137] Seneor, P.; Chen, C.-T.; Yeh, N.-C.; Vasquez, R. P.; Bell, L. D.; Jung, C. U.; Park, Min-Seok ; Kim, Heon-Jung ; Kang, W. N.; Lee, Sung-Ik *Phys. Rev. B* 2001, **65**, 012505.

[138] Koshelev, A. E.; Golubov, A. A. *Phys. Rev. Lett.* 2003, **90**, 177002.

[139] Mazin, I. I.; Andersen, O. K.; Jepsen, O.; Dolgov, O. V.; Kortus, J.; Golubov, A. A.; Kuz'menko, A. B.; van der Marel, D. *Phys. Rev. Lett.* 2002, **89**, 107002.

[140] Ferrando, V.; Tarantini, C.; Manfrinetti, P. ; Marré, D.; Putti, M.; Tumino A.; Ferdeghini, C. In *Applied Superconductivity 2003 - Proc. of VI European Conference on Applied Superconductivity, Sorrento, Italy, 14-18/9/2003*; Andreone, A.; Pepe, G. P.; Cristiano, R.; Masullo, G.; Eds.; Institute of Physics, Conference Series **181**; 2004; pp 1263-1270.

[141] Gurevich, A. *Phys. Rev. B* 2003, **67**, 184515.

[142] Szabó, P.; Samuely, P.; Kacmarcik, J.; Klein, T.; Marcus, J.; Fruchart, D.; Miraglia, S.; Marcenat, C.; Jansen, A. G. M. *Phys. Rev. Lett.* 2001, **87**, 137005.

[143] Dulčić, A.; Paar, D.; Požek, M.; Williams, G. V. M.; Krämer, S.; Jung, C. U.; Park, Min-Seok ; Lee, Sung-Ik *Phys. Rev. B* 2002, **66**, 014505.

[144] Murakami, M.; Sakai, N.; Higuchi, T.; Yoo, S. I. *Supercond. Sci. Technol.* 1996, **9**, 1015.

[145] Küpfer, H.; Wolf, Th.; Zhukov, A. A.; Meier-Hirmer, R. *Phys. Rev. B* 1999, **60**, 7631.

[146] Silva, E.; Pompeo, N. ; Muzzi, L. ; Marcon, R.; Sarti, S. ; Boffa, M. ; Cucolo, A. M. COND-MAT/0405324 (2004).